An adaptive and energy-maximizing control optimization of wave energy converters using an extremum-seeking approach

Physics of Fluids

An adaptive and energy-maximizing control optimization of wave energy converters using an extremum-seeking approach

Cite as: Phys. Fluids **32**, 113307 (2020); https://doi.org/10.1063/5.0028500
Submitted: 05 September 2020 . Accepted: 20 October 2020 . Published Online: 06 November 2020

Luca Parrinello, Panagiotis Dafnakis, Edoardo Pasta, Giovanni Bracco, Peiman Naseradinmousavi, Giuliana Mattiazzo, and Amneet Pal Singh Bhalla

Physics of Fluids ARTICLE scitation.org/journal/phf

An adaptive and energy-maximizing control optimization of wave energy converters using an extremum-seeking approach

Cite as: Phys. Fluids 32, 113307 (2020); doi: 10.1063/5.0028500
Submitted: 5 September 2020 • Accepted: 20 October 2020 •
Published Online: 6 November 2020

Luca Parrinello,[1] Panagiotis Dafnakis,[1] Edoardo Pasta,[1] Giovanni Bracco,[1] Peiman Naseradinmousavi,[2] Giuliana Mattiazzo,[1] and Amneet Pal Singh Bhalla[2,a)]

AFFILIATIONS

[1] Department of Mechanical and Aerospace Engineering, Politecnico di Torino, Turin 10129, Italy
[2] Department of Mechanical Engineering, San Diego State University, San Diego, California 92182, USA

[a)] **Author to whom correspondence should be addressed:** asbhalla@sdsu.edu

ABSTRACT

In this paper, we systematically investigate the feasibility of different extremum-seeking (ES) control and optimization schemes to improve the conversion efficiency of wave energy converters (WECs). Continuous-time and model-free ES schemes based on the sliding mode, relay, least-squares gradient, self-driving, and perturbation-based methods are used to improve the mean extracted power of a heaving point absorber subject to regular and irregular waves. This objective is achieved by optimizing the resistive and reactive coefficients of the power take-off (PTO) mechanism using the ES approach. The optimization results are verified against analytical solutions and the extremum of reference-to-output maps. The numerical results demonstrate that except for the self-driving ES algorithm, the other four ES schemes reliably converge for the two-parameter optimization problem, whereas the former is more suitable for optimizing a single parameter. The results also show that for an irregular sea state, the sliding mode and perturbation-based ES schemes have better convergence to the optimum in comparison to other ES schemes considered here. The convergence of PTO coefficients toward the performance-optimal values is tested for widely different initial values in order to avoid bias toward the extremum. We also demonstrate the adaptive capability of ES control by considering a case in which the ES controller adapts to the new extremum automatically amid changes in the simulated wave conditions. Moreover, no explicit knowledge of (future) wave excitation forces is required in the algorithm, which implies that the model-free ES can be used as a causal controller for WECs. Our results demonstrate that the continuous-time and model-free ES method achieves the optimum within a single simulation, which is in contrast to evolution-based optimization strategies that typically require a large number of (possibly expensive) function evaluations. This makes ES control optimization schemes suitable for nonlinear computational fluid dynamics simulations, where typically evolutionary strategies are used for performing black-box optimization.

I. INTRODUCTION

Renewable energy harvesting technologies have made tremendous progress over the last several decades, which are enabling us to reduce our current carbon footprint of energy production and consumption. In particular, technologies based on wind and solar power are now sufficiently mature and economically viable to be deployed at commercial and utility scales. In contrast, wave energy conversion has yet to achieve a level of commercial success like solar and wind technologies, despite the concerted research efforts dating back since the early 1970s after the oil crisis.[1]

The economy of scale model demonstrated for solar and wind farms motivates future commercial wave farms. For example, the cost of a photovoltaic module dropped from $66.1/W in 1976 to $0.62/W in 2016. Similarly, the levelized cost of electricity generated from wind has significantly decreased over the years, with prices ranging from $0.55/kWh in 1980 to $0.05/kWh in 2012.[2] It is estimated that 2.11 ± 0.05 TW of wave energy is available

globally.[3] Moreover, wave power density is extremely high compared to wind and solar; compare 25 kW/m of crest width for wave energy against 1 kW/m^2 at peak insolation for solar energy or at a wind speed of 12 m/s for wind energy.[4] Despite the favorable attributes, wave power is the most underutilized renewable energy resource.[5] Nevertheless, significant progress has been made in the design and analysis of wave energy converter (WEC) devices, which convert the mechanical energy of the waves to electrical energy through a power take-off (PTO) system.

One of the challenging aspects of making wave energy commercially profitable is designing an optimal controller for a WEC device that maximizes its mean extracted power. Consequently, several optimal control formulations have been proposed in order to improve energy extraction from WECs. An extensive review on this topic can be found in the work of Ringwood *et al.*[6,7] and Maria-Arenas *et al.*[8] One such optimal control formulation is the model-free extremum-seeking (ES) method, which can be applied to both linear and nonlinear systems. ES is an adaptive control that tracks a maximum/minimum (extremum) of a performance/cost function and then drives the output of this function to its extremum.[9] ES control has been used for a variety of applications, including, but not limited to, reducing thermo-acoustic instabilities in gas turbines and rocket engines,[10] flight formation optimization,[11] control of thermo-acoustic coolers,[12] autonomous vehicles[13] and robots,[14] and beam matching in particle accelerators.[15] ES control has also been widely used for wind[16–18] and solar power applications.[19–21] However, only a limited number of ES studies are available for wave energy in the literature.[22,23] The aim of the current study is to fill this gap by testing and comparing different ES control algorithms and demonstrating their feasibility for WECs.

ES control was conceived at the beginning of the twentieth century by Leblanc.[24] The method first received considerable attention in the USSR in the 1940s[25] and then in the Western world in the 1950s and 1960s. Although ES was one of the first forms of adaptive control, it was not until 2000 that a proof of stability for a generic plant was provided by Krstić and Wang.[9] Soon after, many applications and variants of the algorithm followed in the literature. The first application of ES for WECs appeared in 2011 by Hals *et al.*,[23] in which various control strategies, including tuning of controller parameters using perturbation-based ES, were compared through simulation results. Hals *et al.* defined a performance function based on low-pass filters and knowledge of wave excitation forces for tuning linear damping or the threshold value of latching, depending on the controller. The authors compared the controller parameters tuned through gain scheduling and ES strategies in their work.[23] In 2012, Garcia-Rosa *et al.*[22] used a *discrete-time* ES scheme to obtain performance-optimal PTO coefficients of a hyperbaric point absorber converter. In their simulation results, both reactive and resistive coefficients were simultaneously optimized, without requiring the knowledge of wave excitation forces. Similar to Hals *et al.*, the authors in Ref. 22 also used a perturbation-based ES control.

In this work, we use *continuous-time* ES control algorithms to optimize the resistive and reactive PTO coefficients for a heaving point absorber subject to regular and irregular waves. The continuous-time formulation of ES control makes it applicable for different simulation approaches as well, such as within a fully resolved computational fluid dynamics framework. Moreover, our approach also does not require any knowledge of wave excitation forces, which translates to not requiring any wave measuring/forecasting instrument at the site of operation. Furthermore, in contrast to prior works[22,23] that considered only the perturbation-based ES method, we systematically test and compare the performance of the sliding mode,[26] relay,[27] least-squares gradient,[28] self-driving,[29] and perturbation-based[9] ES schemes. The optimization results are verified against analytical solutions and the extremum of reference-to-output maps. The numerical results show that except for the self-driving ES algorithm, the other four ES schemes reliably converge for the two-parameter optimization problem, whereas the former is more suitable for optimizing a single parameter. The results also show that for an irregular sea state, the sliding mode and perturbation-based ES schemes have better convergence to the optimum, in comparison to other ES schemes. The convergence of parameters toward the performance-optimal values is tested for widely different initial values, in order to avoid bias toward the extremum. We also demonstrate the adaptive capability of ES control by considering a case in which the ES controller adapts to the new extremum automatically amid changes in the simulated wave conditions.

There are several advantages to using model-free controllers as opposed to classical model-based controllers such as the linear quadratic regulator (LQR)[30] or model predictive control (MPC)[31] for devices that operate in extreme environments, such as WECs. For example, model-free controllers are able to adapt to various system alterations that may occur during a long-term operation of a WEC device. Typical scenarios include marine growth on the submerged surface, non-critical subsystem failures, and aging/fatigue of internal components of the conversion system. Such alterations are hard to predict or model, but they affect the dynamics of the device significantly over a long period of time. Even if a model is available, it will typically be nonlinear, which rules out linear model-based controllers such as LQR. In contrast, model-free (and nonlinear) controllers such as ES are not affected by modeling errors or uncertainties in the model parameters. Because of these reasons, model-free control schemes, particularly those based on data-driven and machine learning approaches, are becoming increasingly popular in the fluid mechanics community; see, for example, active flow control[32–37] and optimal swimming[38] applications that have utilized deep reinforcement learning (DRL) or genetic programming (GP) based controllers. Data-driven controllers have also been proposed for WECs recently. Anderlini and co-workers have developed control strategies using reinforcement learning[39–41] and artificial neural networks[42] to maximize power absorption of a WEC device. Another example of a machine learning-based controller for WECs can be found in the work of Thomas *et al.* who considered collaborative learning for arrays of WECs in their work.[43]

One of the main drawbacks of model-free control schemes, particularly those based on DRL, is the high computational cost associated with first training the model and then ultimately learning the control policy.[38,44] In contrast, model-free ES controllers rely mostly on perturbation signals, filters, and gradient estimation of the performance function; these operations have much lower computation overhead, which allows ES to be used as an "online" controller/optimizer. Moreover, ES does not rely on the "offline" simulation dataset to optimize the plant behavior, which is an essential

requirement of several machine learning or evolutionary strategy based optimizers. However, modern machine learning controllers using GP techniques enable finding new control laws directly instead of optimizing parameters of traditional control schemes. These developments are relatively recent; see, for example, the work of Duriez *et al.* who used GP for controlling turbulent flows.[35]

The rest of this paper is organized as follows: We begin by stating the assumptions of ES formulation in Sec. II. Next, in Sec. III, we define the performance function for a general energy-harvesting mechanical oscillator and provide a brief overview and working principle of each ES scheme. The equations of motion for bodies oscillating in air and in water are described in Sec. IV. For some cases, the analytical solution to the performance-optimal PTO coefficients is provided. The ES results for a simple mass-spring-damper system oscillating in air and for cylindrical and spherical buoys heaving in regular and irregular waves are provided in Sec. V. Finally, conclusions are drawn in Sec. VI.

II. OVERVIEW OF EXTREMUM-SEEKING CONTROL AND OPTIMIZATION

Extremum-seeking (ES) control is an adaptive optimization technique that derives and maintains the input and output of the controlled plant to their respective extrema without requiring an explicit knowledge of the plant dynamics. ES control can be applied to both linear and nonlinear systems, in which the extremum of a performance function is achieved and maintained by obtaining the gradient information with respect to the control inputs. For the purpose of description, we consider a single-input single-output (SISO) nonlinear system with the following characteristics:

1. an unknown dynamical plant $\dot{x} = f(x,u)$, with $x \in \mathbb{R}^n$ and $u \in \mathbb{R}$;
2. a performance function $J = h(x)$, with $J \in \mathbb{R}$; and
3. a state-feedback control law $u = \alpha(x, \vartheta)$, with $\vartheta \in \mathbb{R}$.

Here, x represents the state of the plant, u is the control input, and J is the performance (cost) metric/function that needs to be maximized (minimized) over a period of time. The function $f(x,u)$ governing the evolution of the plant dynamics is not explicitly required for the ES algorithm. Figure 1 shows a schematic representation of the plant with an embedded ES controller. The following assumptions are made for the extremum-seeking controlled plant:[26,45,47,48]

- **Assumption 1:** The control law $u = \alpha(x, \vartheta)$ is smooth, parameterized by ϑ, and stabilizes the plant.
- **Assumption 2:** There exists a smooth function $x_{eq}(\vartheta)$ such that

$$\dot{x} = f(x, \alpha(\vartheta, x)) = 0 \leftrightarrow x = x_{eq}(\vartheta). \tag{1}$$

- **Assumption 3:** The functions $f : \mathbb{R}^n \times \mathbb{R} \longrightarrow \mathbb{R}^n$ and $h : \mathbb{R}^n \longrightarrow \mathbb{R}$ are smooth.
- **Assumption 4:** The static performance behavior of the system at the equilibrium point $x_{eq}(\vartheta)$ can be expressed by

$$J_{eq} = h(x_{eq}(\vartheta)) = F(\vartheta), \tag{2}$$

in which $F(\vartheta)$ is a smooth function and admits a unique maximum or minimum at $\vartheta = \vartheta^*$.

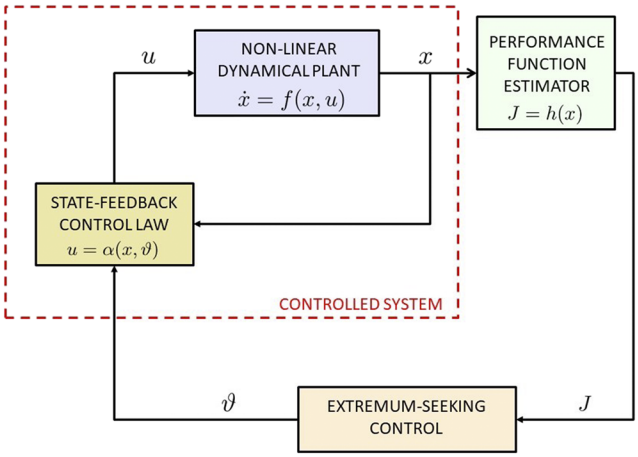

FIG. 1. Extremum-seeking control scheme for a general SISO nonlinear system.[45,46]

- **Assumption 5:** The parameter ϑ evolves much slower than the dynamics of the plant; the latter is assumed to be in equilibrium [Eq. (1)]. Thus, we can omit the dynamics of the plant while analyzing ES control. Given these operating conditions, we are aiming toward achieving a steady-state optimization of the plant. It then follows that the time derivative of the performance function of the *stabilized plant* can be expressed as

$$\dot{J}_{eq} = \frac{dJ_{eq}}{dt} = \frac{dJ_{eq}}{d\vartheta}\frac{d\vartheta}{dt} = \frac{dF(\vartheta)}{d\vartheta}\dot{\vartheta}. \tag{3}$$

Under the same set of aforementioned assumptions, it is also possible to extend the ES analysis to a multiple-input single-output (MISO) system, in which $\vartheta \in \mathbb{R}^m$. The objective here is to optimize m parameters simultaneously. For the stability analysis of ES control of a SISO system, we refer the readers to Ref. 9, and for that of a MISO system, the readers are referred to Refs. 13, 14, and 49–53.

III. EXTREMUM-SEEKING CONTROL ALGORITHMS

In this work, we use *model-free* ES (also referred to as *black-box* ES) algorithms to enhance the power absorption of periodically oscillating systems, such as wave energy converter devices. The ES algorithms used in this work belong to the class of *derivative-based* optimization methods, which aim to determine the optimal value of the performance function J by estimating the derivative $dJ/d\vartheta$ to obtain the value ϑ^* that maximizes (minimizes) the performance (cost) function. Extremum-seeking control problems are typically formulated as unconstrained optimization problems, as done in this work and in prior works that used ES for WECs.[22,23] In order to include inequality constraints on the plant parameters, the performance/cost function can be augmented with penalty functions.[54,55] However, constraints on the state variables and performance indicators cannot be imposed in general because the state of the plant and an explicit relationship between plant parameters and performance indicators is not known *a priori*. Since a model-free ES algorithm

is oblivious to the underlying system dynamics, its success depends upon the definition of the performance function, which the control designer is free to define. For energy harvesting systems, a natural choice of performance function is the amount of energy absorbed by the device over a period of time. An ES algorithm then finds the maxima of this concave (performance) function with respect to the PTO parameters.

The performance/cost function defined for an ES algorithm should be time-invariant, and remain constant, if the parameter ϑ remains constant.[29] During the steady-state operation of a WEC device, the absorbed energy is a time-varying periodic function with a non-zero mean. Therefore, it is important to work with mean powers rather than instantaneous powers in the performance function, in order to satisfy assumption 5 given in Sec. II. In this work, we define the mean of the absorbed power over a couple of wave periods. There are two advantages of using this definition: (i) first, it ensures that the device dynamics are much faster than the performance function variation and (ii) second, ES control remains adaptive in the presence of changing wave conditions. The adaptive capability of ES is maintained because typically the wave climate changes over several hundred wave periods, while the performance function is (re-)defined over the last few (wave) periods.

Specifically in this work, the performance function J for ES algorithms is defined to be a composite function of the instantaneous power $P(t)$ absorbed by the PTO unit, as shown in Fig. 2. The composition consists of (i) a low-pass filter (LPF), (ii) a moving average defined over last few wave periods, and (iii) a logarithmic function. Depending upon the type of PTO machinery, the instantaneous power $P(t)$ could be only resistive in nature (resistive meaning that the PTO absorbs power from the waves and sends it to the electric grid one way), or it could have both resistive and reactive (reactive meaning that PTO can also withdraw power from the grid and inject it into the device at times to invoke optimal phase control) power components. Irrespective of the PTO type, the power signal $P(t)$ is characterized by two main frequency types: the first, which is at a higher value, is characterized by the fast dynamics of the plant itself and the second, at a lower value, is characterized by the slow variation of the parameter ϑ provided by ES. The purpose of the low-pass filter is to eliminate the higher frequency content from the performance metric, while that of the moving average is to evaluate the steady-state performance of the plant (see Ref. 29 for more discussion). The signal μ, which is the output of the first two operators, can be used to assess the device performance as a function of ϑ parameter. However, the plant or the device could be operating under wide variability of conditions (such as changing wave heights or periods), and the resulting power can vary in different orders of magnitude. As suggested by Ciri *et al.*,[56] the purpose of the logarithmic function is to limit the variation of the performance metric drastically, which reduces the sensitivity of the controller response and avoids re-tuning ES controller parameters for changing operating conditions of the plant. This can also be observed in Fig. 2(b), which compares the scale of oscillation of various functions involved in the performance function estimator block.

Next, we discuss and describe different ES algorithms used in this paper and make some recommendations on the controller parameters of the ES algorithms.

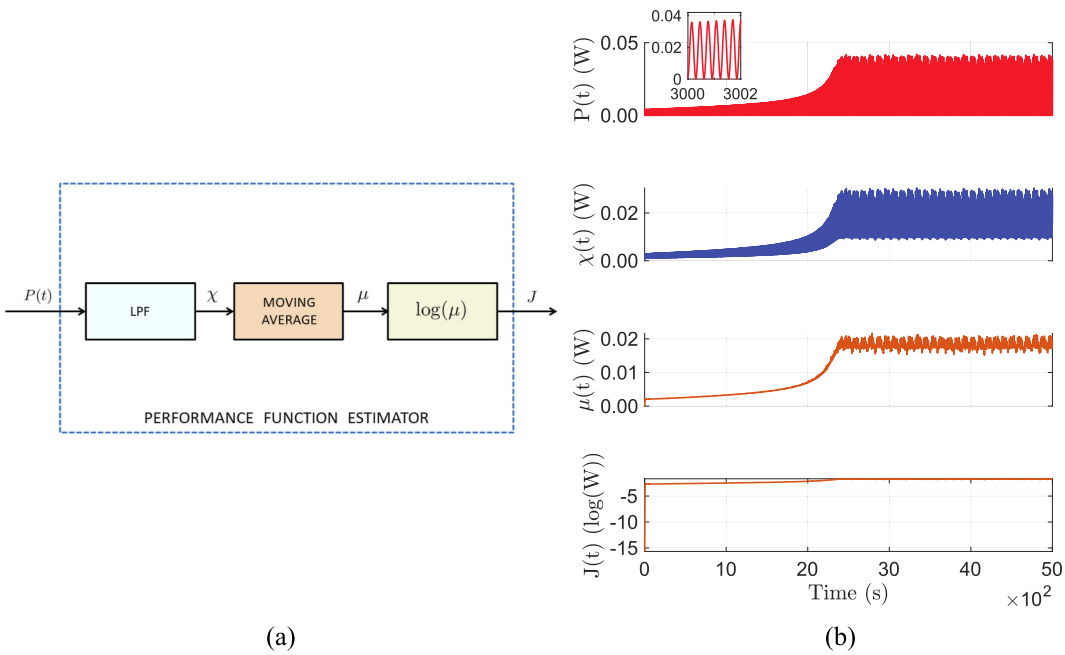

FIG. 2. (a) Block-diagram scheme to obtain the performance function J for ES algorithms using instantaneous power $P(t)$ absorbed by the PTO unit. A first-order low-pass filter of the form $\frac{\omega_L}{s+\omega_L}$ is used, in which ω_L is the cutoff frequency. (b) Representative time evolution of various functions during a WEC operation: $P(t)$, $\chi(t)$, $\mu(t)$, and $J(t)$.

A. Sliding mode extremum-seeking control

The basic idea of the sliding mode extremum-seeking control (SM-ES) is to make the performance function J follow an increasing function of time $q(t)$, irrespective of the unknown gradient $\mathrm{d}J/\mathrm{d}\vartheta$ via sliding mode motions. The error signal $\varepsilon = J(\vartheta) - q(t)$ is then kept at a constant value by a proper choice of $\dot{\vartheta}$ (via the sliding mode) given by

$$\dot{\varepsilon} = \frac{\mathrm{d}J}{\mathrm{d}\vartheta}\dot{\vartheta} - \dot{q}(t), \tag{4}$$

$$\dot{\vartheta} = \mathcal{K}\tanh(\sin(\varepsilon\pi/\beta)), \quad \mathcal{K} > 0. \tag{5}$$

Figure 3 shows a block diagram of the sliding mode ES control system. Equivalently, the SM-ES can be described by the following set of equations:

$$\text{SM-ES} = \begin{cases} \dot{q} = \varrho, & \varrho > 0, \\ \varepsilon = J - q, & \\ \xi = \tanh(\sin(\varepsilon\pi/\beta)), & \beta > 0, \\ \dot{\vartheta} = \mathcal{K}\xi, & \mathcal{K} > 0. \end{cases} \tag{6}$$

For more details on SM-ES, including its stability analysis and recommendations for tuning its parameters, we refer the readers to Refs. 26, 27, and 57. Below, we list some key recommendations followed in this work:

- The ratio $\beta\mathcal{K}/2\varrho$ affects the convergence rate to attain the performance-optimum value ϑ^*. A value too small slows down the convergence rate, whereas an extremely large value can be detrimental to the system stability.
- $\varrho/\mathcal{K}$ and β have to be chosen small to ensure the stability and convergence of the algorithm.
- To satisfy assumption 5 of Sec. II, i.e., the variation of the parameter ϑ needs to be much slower than the dynamics of the plant, the controller parameters $\mathcal{K}$ and ϱ need to be smaller than β. Our empirical tests suggest that the ratio β/ϱ approximately equal to 10^2 ensures the stability and convergence of the algorithm.

B. Relay extremum-seeking control

A relay extremum-seeking control[27] provides an estimation of the plant optimum based on the sign of the gradient. This feature is particularly useful when the controller is applied to a plant operating under widely varying conditions, which can cause the gradient value to vary in different orders of magnitude, as discussed in Sec. III. In this case, using a logarithmic function in the functional composition of the performance metric is redundant, and the performance metric μ (instead of J) can be used directly for the relay ES. However, a drawback of discarding the gradient magnitude is that the parameter ϑ keeps oscillating in the neighborhood of the optimal value ϑ^*, where the gradient norm is $|\mathrm{d}\mu/\mathrm{d}\vartheta|_{\vartheta^*} \approx 0$. Nevertheless, acceptable oscillations can be achieved with a proper tuning of the relay ES controller parameters.[27] Figure 4 shows a block diagram of the relay ES control system, which is described by the following set of equations:

$$\text{Relay ES} = \begin{cases} g = \frac{\delta\mu}{\delta\vartheta}, & \\ \xi = \xi_0\ \mathrm{signum}(g), & \xi_0 > 0, \\ \dot{\hat{\vartheta}} = \xi, & \\ \vartheta = \hat{\vartheta} + a_\mathrm{p}\sin(\omega_\mathrm{p}t), & a_\mathrm{p} > 0, \end{cases} \tag{7}$$

in which $\delta\mu/\delta\vartheta$ is the estimation of the gradient $\mathrm{d}\mu/\mathrm{d}\vartheta$ obtained using a least-squares gradient estimation method, and the quantity $\Delta_\mathrm{p}(t) = a_\mathrm{p}\sin(\omega_\mathrm{p}t)$ is a small perturbation/dither added to the parameter ϑ in order to avoid numerical issues related to the least-squares gradient estimation.[28] The gradient g estimation is performed by generating two buffers of length n_buff, which contain the last n_buff values of performance metric μ and parameter ϑ, as shown in Fig. 5. Given these two buffers, it is possible to estimate $\mathrm{d}\mu/\mathrm{d}\vartheta$ through applying the least-squares method, as explained in Ref. 28. A proof of stability for the relay ES method is provided in Ref. 58.

Since the gradient estimation of the performance function is performed without a dither signal (as done in classical *perturb and observe* ES methods), the convergence speed of relay ES does not depend on the time scale of the external perturbation signal, which potentially allows for a faster convergence of relay ES systems. The signum function in Eq. (7) is defined as

$$\mathrm{signum}(g) = \begin{cases} 1 & \text{if} \quad g \geq 0 \\ -1 & \text{if} \quad g < 0. \end{cases} \tag{8}$$

The above definition of the signum function implies that the algorithm keeps oscillating in the neighborhood of the optimal value ϑ^*, as discussed earlier. Therefore, the choice of the controller parameter ξ_0 is important; ξ_0 should be selected large enough to grant an appreciable variation of the parameter ϑ, which helps accelerate the

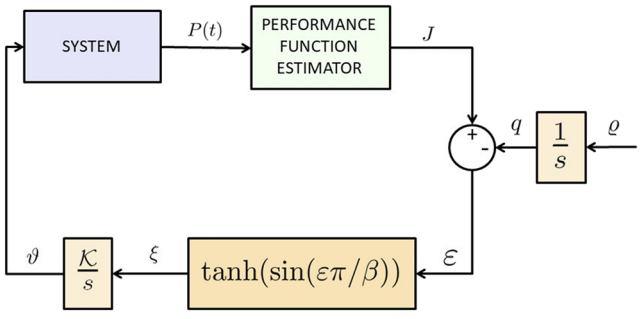

FIG. 3. Block diagram of the sliding mode extremum-seeking control system.[26]

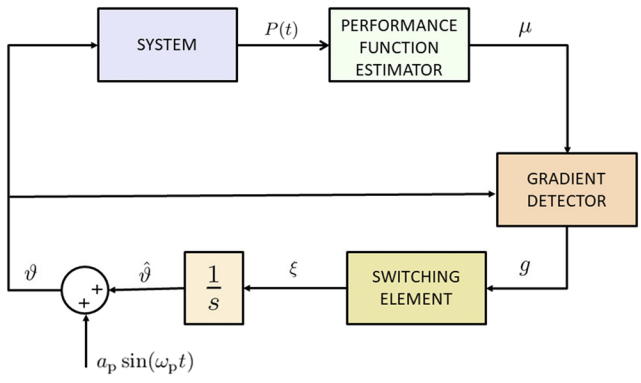

FIG. 4. Block diagram of the relay extremum-seeking control system.[27]

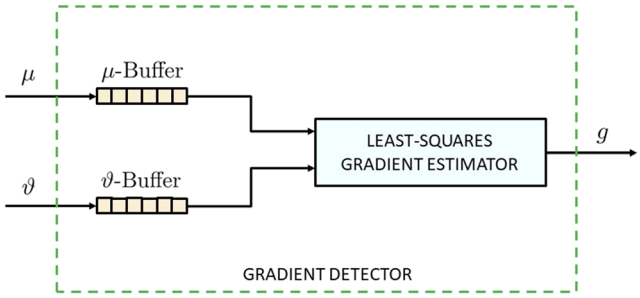

FIG. 5. Least-squares gradient estimation for relay ES.

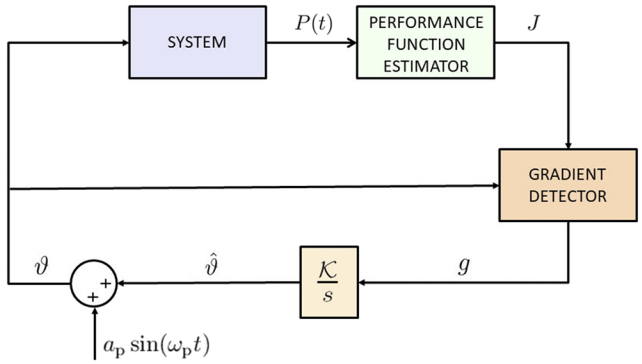

FIG. 6. Block diagram of the least-squares gradient estimation-based extremum-control system.[28]

convergence of the algorithm. However, an extremely large value of ξ_0 causes excessive oscillations and possibly numerical instabilities. Hence, a suitable value of ξ_0 should be found empirically.

In our empirical testing, we observed that adopting an excessively small buffer size makes the controller more reactive but also much more sensitive to the selection of controller parameters (empirical test data not shown). On the contrary, using large buffer size makes the controller less reactive and leads to a poor estimation of the gradient. The size of the buffer also depends on the time step size adopted for acquiring data; if the step size is extremely small, the buffers need to be larger and vice versa. In our tests, we maintain a buffer size sufficient enough to store the history of system performance over the last few (typically two) wave periods. We remark that for the algorithm to converge during the initial phase of the simulation, we initialize ϑ-buffer with some non-constant values and keep the controller inactive. The μ-buffer is filled as the simulation proceeds forward within this initial phase.

The controller parameters a_p and ω_p of the sinusoidal perturbation should be set such that the time scale of the perturbation is larger than the time scale of the plant; ω_p must be chosen small enough for this reason. The perturbation amplitude a_p is also kept small to preserve the stability of the ES algorithm, as well as to reduce the oscillations around the performance-optimal value ϑ^*. In contrast, if the a_p value is too small, then inaccuracies stemming from the least-squares gradient estimation can cause a numerical instability.

C. Least-squares extremum-seeking control

The least-squares gradient estimation-based extremum-seeking control algorithm (LSQ-ES) is an extension of the relay ES, in which both the sign and magnitude of the gradient of the performance function estimate $\mathrm{d}J/\mathrm{d}\vartheta$ is used to derive ϑ to its performance-optimal value. A block diagram of the LSQ-ES control system is shown in Fig. 6. The algorithm is equivalently described by the following set of equations:

$$\text{LSQ-ES} = \begin{cases} g = \frac{\delta J}{\delta \vartheta}, & \\ \dot{\hat{\vartheta}} = \mathcal{K} g, & \mathcal{K} > 0, \\ \vartheta = \hat{\vartheta} + a_p \sin(\omega_p t), & a_p > 0, \end{cases} \tag{9}$$

in which $\delta J/\delta\vartheta$ is the least-squares gradient estimation of the performance function $\mathrm{d}J/\mathrm{d}\vartheta$, as described in Ref. 28. Here, we use J instead of μ as a performance metric, for reasons discussed previously.

The stability analysis of LSQ-ES performed in Ref. 28 shows that the parameter $\mathcal{K}T$ affects the algorithmic performance; $\mathcal{K}T$ should be chosen small enough to guarantee the convergence and stability of the algorithm. Here, the controller parameter $\mathcal{K}$ is the gain of the integrator as written in Eq. (9), and T is the time period over which the input and output signals are stored in the data buffers. Therefore, $\mathcal{K}$ should be adjusted according to the duration of the time period T. As LSQ-ES is based on the relay ES algorithm, the remaining controller parameters should be selected as per Sec. III B.

D. Self-driving extremum-seeking control

A self-driving extremum-seeking control scheme, such as the sliding mode extremum-seeking control, does not require perturbations to estimate the gradient of the performance function. As no perturbations are used, the algorithm avoids the time scale associated with the perturbations, which may potentially allow for a faster convergence toward the optimum. Although self-driving systems were part of the ES algorithms surveyed by Sternby[59] in 1980, they have since not gained much popularity compared to the perturbation-based ES methods. However, lately, they are receiving a renewed attention in the literature; see Ref. 29 and references therein. Here, we follow Haring to present a block diagram of a self-driving ES control system, as shown in Fig. 7. The controller can be equivalently described by the following set of equations:

$$\text{Self-driving ES} = \begin{cases} \dot{m}_1 = \eta(J - m_1), & \eta > 0, \\ \dot{m}_2 = \eta Q_1 Q_2 (J - m_1 - Q_1 m_2) - \sigma\eta Q_2 m_2, & \sigma \geq 0, \\ \dot{Q}_1 = -\eta Q_1 + \dot{\vartheta}, & \\ \dot{Q}_2 = \eta Q_2 - \eta Q_1^2 Q_2^2 - \sigma\eta Q_2^2, & \\ \dot{\vartheta} = \lambda\eta m_2, & \lambda > 0. \end{cases} \tag{10}$$

Succinctly, the *observer* block estimates the gradient of the performance function, $m_2 \approx \mathrm{d}J/\mathrm{d}\vartheta$, and the *optimizer* block steers the

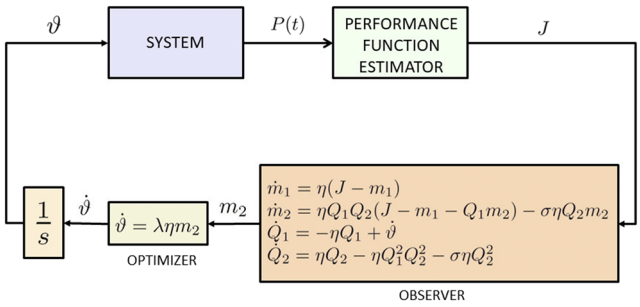

FIG. 7. Block diagram of the self-driving extremum-seeking control system.[29]

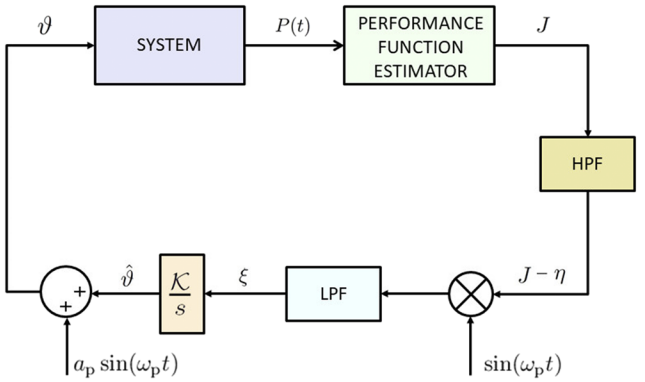

FIG. 8. Block diagram of the perturbation-based extremum-seeking control system.[45] First-order low-pass and high-pass filters of the form $\frac{\omega_L}{s+\omega_L}$ and $\frac{s}{s+\omega_H}$, respectively, are used.

parameter ϑ toward the performance-optimal value ϑ^*. A peculiarity of this approach is that, instead of using perturbation/dither signals, the self-driving ES method uses three auxiliary functions Q_1, Q_2, and m_1 to estimate the gradient of the performance function. As discussed in Ref. 29, if $m_2(t = 0)$ and $Q_1(t = 0)$ are equal to zero, the parameter ϑ will remain constant, and not converge to the optimal value. In our simulations, we initialize $m_2(0)$ and $Q_1(0)$ with $\mathcal{O}(1)$ values and evolve them for a sufficiently long period of time, during which the controller is kept inactive. In addition, to accelerate the convergence rate, higher values of the controller parameters λ and η should be chosen. However, if these are excessively high, stability issues may occur. Numerical instabilities may also arise due to high values of Q_2 during the simulation; it is recommended to regularize Q_2 through a non-zero σ value, as shown in the set of equations (10). Since larger values of σ can compromise the accuracy of the performance-optimal ϑ^*, we set $\sigma \approx 10^{-11}$ in our simulations. For details on the working principle of a self-driving ES method, we refer the readers to Ref. 29.

Through our empirical tests done for the cases studied in this work, we find that the self-driving algorithm as is described in this section does not converge well for MISO systems. However, for SISO systems, the convergence toward the optimum solution is reasonably fast and free of oscillations.

E. Perturbation-based extremum-seeking control

Perturbation-based extremum-seeking control is historically the first ES control algorithm. In 1922, Leblanc first applied a perturbation-based ES to maximize the power transfer from an overhead electrical transmission line to a tram car.[24] The method underwent several extensions and modifications until 1960s, after which it had lost popularity *in lieu* of other control schemes at that time. This was mainly because of the difficulty to generalize the algorithm for a large class of plants. In 2000, Krstić and Wang[9] proved the stability of the perturbation-based extremum-seeking control scheme for a generic plant satisfying certain properties, as listed in Sec. II. This publication has reignited the interest of the research community in ES methods, and since then, many variants and applications based on extremum-seeking control algorithms have been considered—some of which were discussed in Secs. III A–III D. Figure 8 shows a block diagram of the perturbation-based ES control system. The scheme can be equivalently described by the following set of equations:

$$\text{Perturbation-based ES} = \begin{cases} \dot{\eta} = \omega_H(J - \eta), & \omega_H > 0, \\ \dot{\xi} = \omega_L((J - \eta)\sin(\omega_p t) - \xi), & \omega_L > 0, \\ \dot{\hat{\vartheta}} = \mathcal{K}\xi, & \mathcal{K} > 0, \\ \vartheta = \hat{\vartheta} + a_p \sin(\omega_p t). & a_p > 0. \end{cases} \tag{11}$$

An intuitive working principle of perturbation-based ES can be explained as follows. A perturbation signal $\Delta_p(t) = a_p \sin(\omega_p t)$ is added to the current estimate of the parameter ϑ and passed into the plant. The plant's performance J is measured/calculated for the updated parameter. If the output signal J can be linearized around the current estimate of ϑ, then the change in J due to the perturbation signal can be obtained using a Taylor series expansion

$$J - \eta \approx \frac{dJ}{d\vartheta}\Delta_p, \tag{12}$$

in which η is the DC component of the signal that can be subtracted from J by passing it through a high-pass filter (HPF) of cutoff frequency ω_H. The change in the performance function due to the added perturbation is then multiplied by another perturbation signal to yield the following quantity:

$$(J - \eta)\Delta_p \approx \frac{dJ}{d\vartheta}\Delta_p^2. \tag{13}$$

The resultant of this operation is passed through a low-pass filter (LPF) of cutoff frequency ω_L, which extracts the (slowly varying) performance gradient $\xi \approx dJ/d\vartheta$ with the correct sign. (As Δ_p^2 is a positive quantity, the sign of the signal is decided by the gradient of the performance function $dJ/d\vartheta$.) Following the gradient estimation, an integrator with gain $\mathcal{K}$ updates the ϑ parameter, and the optimization process is repeated until convergence is obtained.

The amplitude a_p of the perturbation and the gain $\mathcal{K}$ of the integrator should be chosen small enough to guarantee convergence, as discussed in Refs. 9 and 60. Moreover, the smaller value of a_p reduces

oscillation of ϑ in the neighborhood of the performance-optimal value ϑ^*. The angular frequency ω_p of the dither signal should be lower than the plant frequency, in order to satisfy assumption 5 given in Sec. II.

IV. EQUATIONS OF MOTION

In this section, we describe the equations of motion of energy-harvesting mechanical oscillators operating in air and in water environments. A mechanical oscillator working in air is also referred to as a "dry" oscillator in the wave energy literature.[61] Although the objective of the current work is to maximize the power extraction of point absorber devices using extremum-seeking control, an analytical solution to the dry oscillator problem is available, which can be used to validate the optimal solution obtained using ES. Moreover, there is a direct equivalence between the performance optimal PTO coefficients of a dry oscillator and a WEC subject to regular waves, which further justifies considering the dry oscillator problem first.

A. Bodies oscillating in air

The equation of motion of a single degree of freedom spring-mass-damper system oscillating in air and subject to an external periodic force of frequency ω reads as

$$m\ddot{x}(t) + c\dot{x}(t) + kx(t) = f_e(t) + f_{PTO}(t), \tag{14}$$

in which m is the mass of the oscillator, c is the damping coefficient, k is the spring stiffness coefficient, and x is the upward heaving direction; see Fig. 9(a). The external periodic force f_e and the control force f_{PTO} applied through the power take-off unit are taken to be of the form

$$f_e(t) = f_0 \sin(\omega t), \tag{15}$$

$$f_{PTO}(t) = -Kx(t) - C\dot{x}(t), \tag{16}$$

in which f_0 is the amplitude of the external force, and a proportional-derivative (PD) control law is used for the control force. [It is also possible to have an inerter integrated into the PTO system so that $f_{PTO}(t) = -Kx(t) - C\dot{x}(t) - A\ddot{x}$, in which A is the inertance coefficient of the PTO; see Ref. 62.] Using impedance-matching or complex-conjugate control analysis, it can be shown that the average-power

$$\bar{P} = \frac{1}{\mathcal{T}}\int_t^{t+\mathcal{T}} C\dot{x}^2 \, dt \tag{17}$$

extracted from the system over a time period $\mathcal{T} = 2\pi/\omega$ is maximal, when the system is in resonance with the external forcing. In other words, when the natural frequency of the system ω_n equals the external frequency ω, the extracted power is maximized. Since it is inconvenient or often times impossible to change the inherent characteristics of the system (m, c, k), the PD control law allows the control designer to adjust the reactive and resistive PTO coefficients, K and C, respectively, to optimize the system performance for varying external forces and disturbances. The energy-maximizing PTO parameters (in the absence of disturbances) can be found analytically as[63]

$$K_{opt} = \omega^2 m - k, \tag{18}$$

$$C_{opt} = c. \tag{19}$$

In Sec. V A, we make use of Eqs. (18) and (19) to verify the optimal solutions $K(\vartheta_1^*)$ and/or $C(\vartheta_2^*)$ obtained using ES.

We remark that in some other optimal control formulations, for example, in model predictive control of converters,[31] the objective is to find the energy-maximizing control force f_{PTO} directly. The average-power extracted by the system over a time period $\mathcal{T}$ is expressed as

TABLE I. Sea states.

Regular sea ID	$\mathcal{T}$(s)	$\mathcal{H}$ (m)	Irregular sea ID	$\mathcal{T}_p$ (s)	$\mathcal{H}_s$ (m)
Reg.1	0.625	0.01	Irreg.1	0.625	0.01
Reg.2	0.8	0.02	Irreg.2	0.8	0.02
Reg.3	1.0	0.0075	Irreg.3	1.0	0.0075

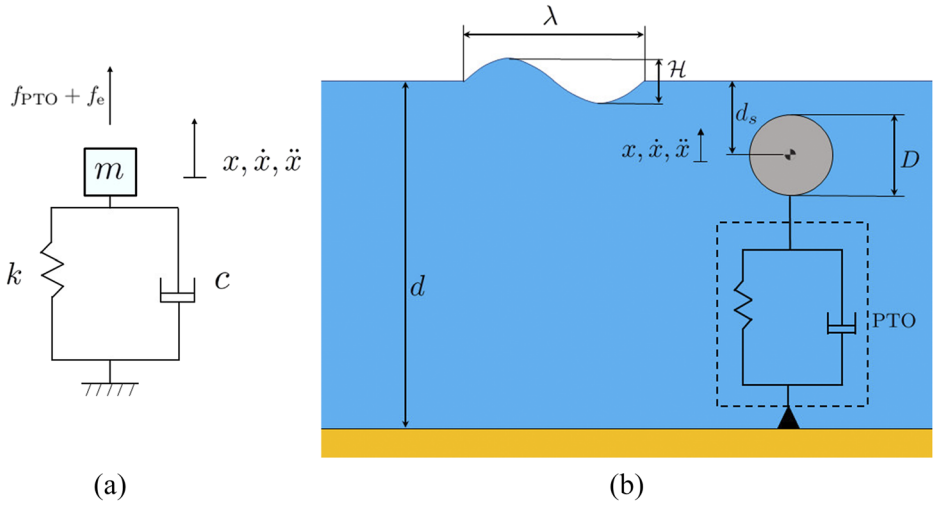

FIG. 9. Schematic of an energy-harvesting (a) mass-spring-damper system and (b) a fully submerged point absorber wave energy converter.

TABLE II. Mass-spring-damper parameters.

Parameter	Value
m (kg)	18.55
k (N/m)	200
c (N s/m)	15
$\mathcal{T}$(s)	0.5
f_0 (N)	10
K_{opt} (N/m)	2729
C_{opt} (N s/m)	15

$$\tilde{P} = \frac{1}{\mathcal{T}} \int_t^{t+\mathcal{T}} -f_{\text{PTO}}\, \dot{x}\, \mathrm{d}t. \tag{20}$$

For a PD control law, Eq. (20) is equivalent to Eq. (17),

$$\begin{aligned} \tilde{P} &= \frac{1}{\mathcal{T}} \int_t^{t+\mathcal{T}} -f_{\text{PTO}}\, \dot{x}\, \mathrm{d}t \\ &= \frac{1}{\mathcal{T}} \int_t^{t+\mathcal{T}} (Kx + C\dot{x})\dot{x}\, \mathrm{d}t \\ &= \frac{1}{\mathcal{T}} \int_t^{t+\mathcal{T}} K \frac{\mathrm{d}}{\mathrm{d}t}\left(\frac{x^2}{2}\right) \mathrm{d}t + \frac{1}{\mathcal{T}} \int_t^{t+\mathcal{T}} C\dot{x}^2\, \mathrm{d}t, \end{aligned} \tag{21}$$

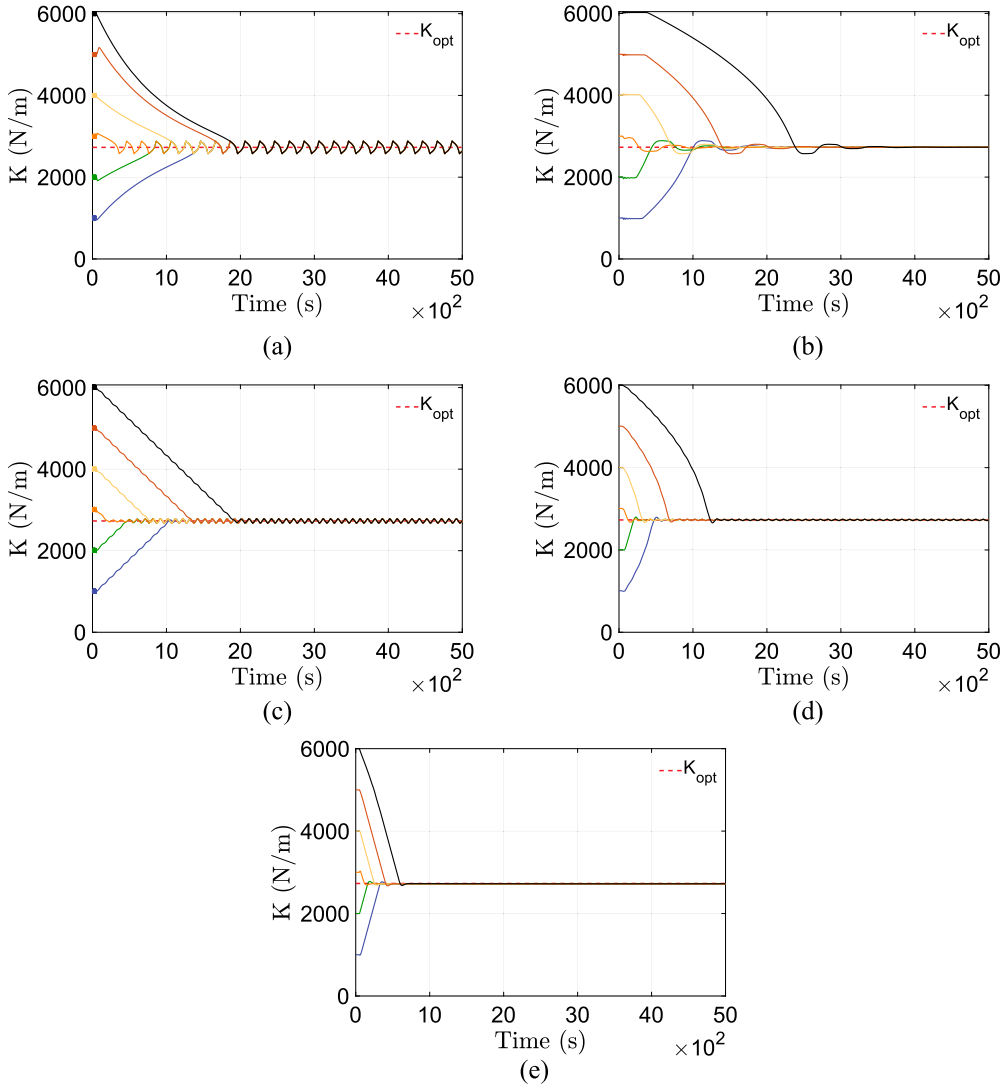

FIG. 10. Optimization of the reactive coefficient K at a fixed value of resistive coefficient $C = C_{\text{opt}}$ for the mass-spring-damper system using (a) sliding mode, (b) self-driving, (c) relay, (d) LSQ, and (e) perturbation-based ES algorithms. The optimal $K_{\text{opt}} = 2729$ N/m value is indicated by the dashed line in the plots.

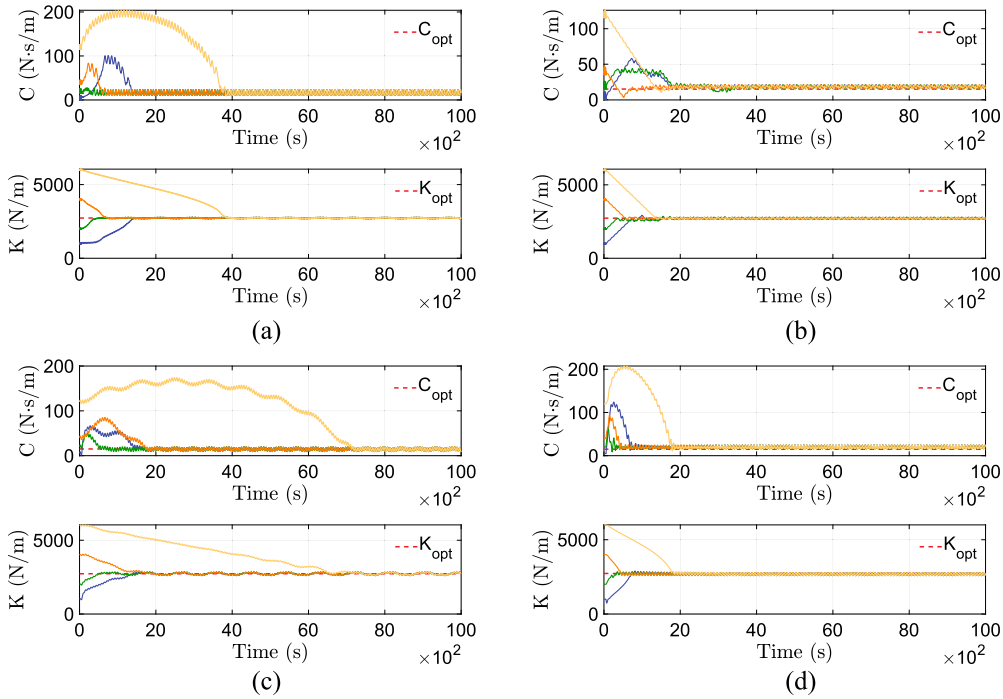

FIG. 11. Optimization of reactive and resistive coefficients, K and C, respectively, for the mass-spring-damper system using (a) sliding mode, (b) relay, (c) LSQ, and (d) perturbation-based ES algorithms. The optimal K_{opt} = 2729 N/m and C_{opt} = 15 N s/m values are indicated by dashed lines in the plots.

as the first term in Eq. (21) vanishes under the time-periodic motion of the device. Appendix A numerically verifies that the inclusion of the reactive component of power in the performance function does not affect the final optimized values of PTO coefficients using ES. Therefore, we use only the resistive component of power or Eq. (17) for defining the performance function.

B. Bodies oscillating in water

The equation of motion of a fully submerged point absorber with a single degree of freedom [see Fig. 9(b)] reads as

$$m\ddot{x}(t) = f_w(t) + f_r(t) + f_v(t) + f_{PTO}(t), \tag{22}$$

in which m is the mass of the point absorber, f_w is the wave excitation force (Froude–Krylov and diffraction), f_r is the radiation force, f_v

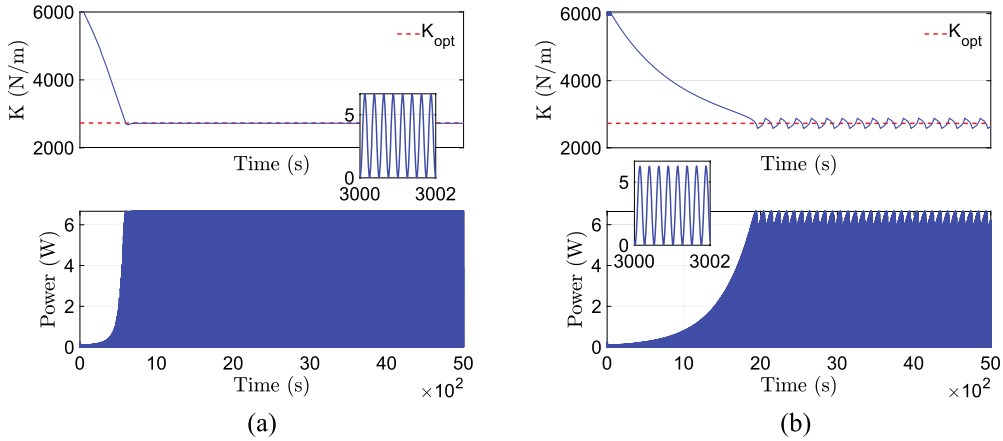

FIG. 12. Extracted power $P(t)$ during reactive coefficient optimization using (a) perturbation-based ES and (b) sliding mode ES.

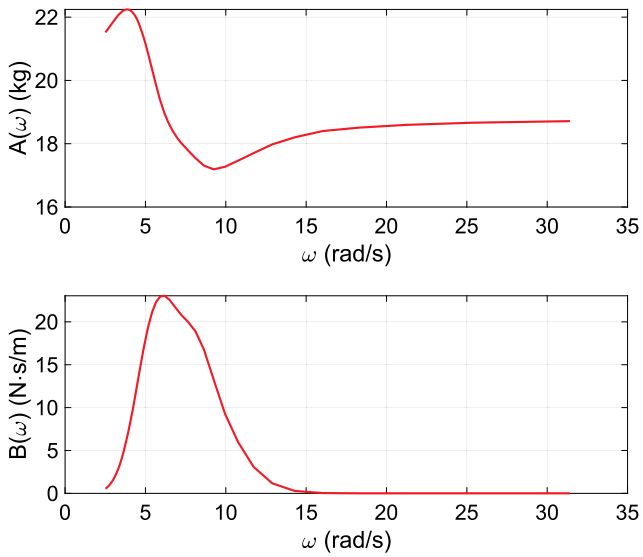

FIG. 13. Frequency-dependent added-mass $A(\omega)$ and radiation damping $B(\omega)$ for the two-dimensional cylindrical buoy. The coefficients are obtained using BEM-based ANSYS AQWA software.

is the viscous drag force, and f_{PTO} is the PD control force applied by the PTO mechanism, as given in Eq. (16). The physical origin of radiation force stems from the energy dissipation mechanism of a moving body that emanates waves during its motion in water. Using the Cummins equation,[64] the radiation force is expressed as

$$f_{\mathrm{r}}(t) = -A_{\infty}\ddot{x} - \int_0^t h_{\mathrm{r}}(t-\tau)\dot{x}(\tau)\,\mathrm{d}\tau, \tag{23}$$

in which A_{∞} is the infinite-frequency added mass and $h_{\mathrm{r}}(t)$ is the radiation impulse response function that contains the fluid-memory effect. The radiation force can also be obtained from the inverse Fourier transform of $H_{\mathrm{r}}(j\omega)$,

$$H_{\mathrm{r}}(j\omega) = B(\omega) + j\omega(A(\omega) - A_{\infty}), \tag{24}$$

$$h_{\mathrm{r}}(t) = \frac{1}{\pi}\int_0^{\infty} H_{\mathrm{r}}(j\omega)e^{j\omega t}\,\mathrm{d}\omega, \tag{25}$$

in which the frequency-dependent added mass $A(\omega)$, and the frequency-dependent radiation damping $B(\omega)$, can be obtained using boundary element method (BEM)-based codes such as WAMIT[65] or ANSYS AQWA.[66] For computational efficiency, as well as for representational convenience, the radiation convolution integral in Eq. (23) can be approximated by an equivalent state-space formulation[67,68]

$$\begin{aligned} k_{\mathrm{r}}(t) &= \int_0^t h_{\mathrm{r}}(t-\tau)\dot{x}(\tau)\,\mathrm{d}\tau \\ &\simeq \begin{cases} \dot{\boldsymbol{\zeta}}_{\mathrm{r}}(t) = \boldsymbol{\mathcal{A}}_{\mathrm{r}}\boldsymbol{\zeta}_{\mathrm{r}}(t) + \boldsymbol{\mathcal{B}}_{\mathrm{r}}\dot{x}(t), & \boldsymbol{\mathcal{A}}_{\mathrm{r}} \in \mathbb{R}^{n_{\mathrm{r}}\times n_{\mathrm{r}}}, \boldsymbol{\zeta}_{\mathrm{r}} \in \mathbb{R}^{n_{\mathrm{r}}\times 1} \\ k_{\mathrm{r}}(t) = \boldsymbol{\mathcal{C}}_{\mathrm{r}}\boldsymbol{\zeta}_{\mathrm{r}}(t), & \boldsymbol{\mathcal{C}}_{\mathrm{r}} \in \mathbb{R}^{1\times n_{\mathrm{r}}}, \end{cases} \end{aligned} \tag{26}$$

in which $\boldsymbol{\mathcal{A}}_{\mathrm{r}}, \boldsymbol{\mathcal{B}}_{\mathrm{r}}$, and $\boldsymbol{\mathcal{C}}_{\mathrm{r}}$ are the state-space matrices and n_{r} is the approximation-order of $H_{\mathrm{r}}(j\omega)$ in the frequency-domain or $h_{\mathrm{r}}(t)$ in the time-domain. In this work, we also follow the state-space

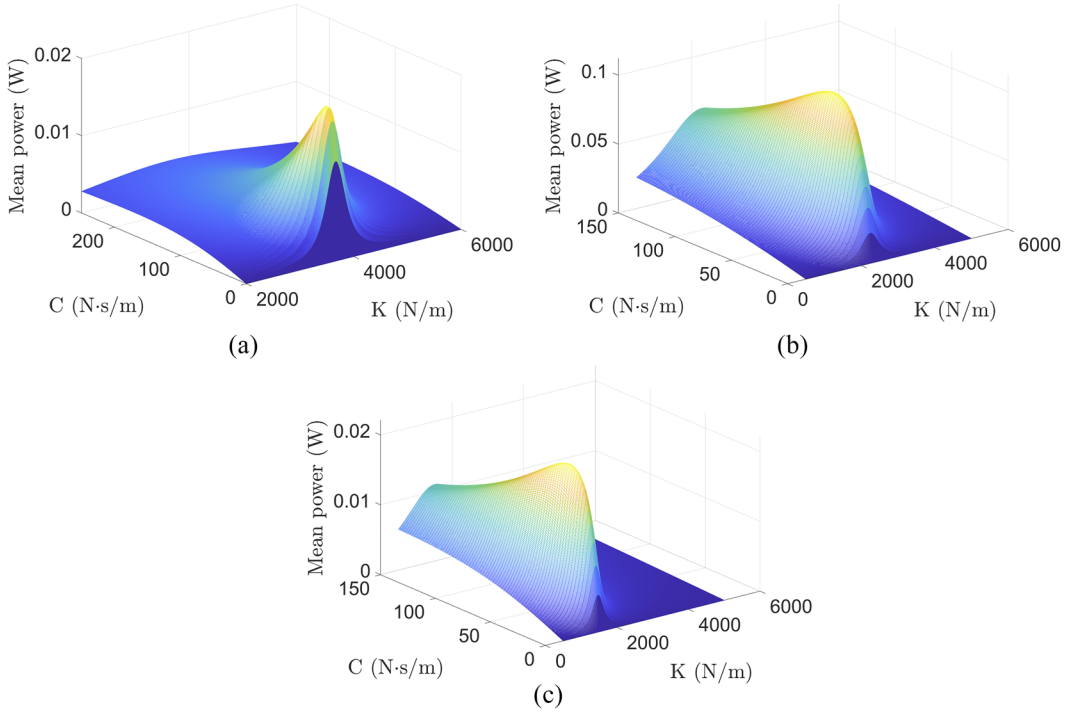

FIG. 14. Power vs PTO coefficient reference-to-output map for a two-dimensional cylinder subject to regular waves. The optimal PTO coefficients are (a) K_{opt} = 3720 N/m and C_{opt} = 18 N s/m; (b) K_{opt} = 2290 N/m and C_{opt} = 34 N s/m; and (c) K_{opt} = 1530 N/m and C_{opt} = 30 N s/m.

TABLE III. Optimal PTO coefficients for a two-dimensional cylindrical buoy subject to regular waves using impedance-matching control theory and through a brute-force search. Units: $\mathcal{T}$ is in s, $\mathcal{H}$ is in m, K is in N/m, and C is in N s/m.

Sea state ID	$\mathcal{T}$	$\mathcal{H}$	$K_{\text{opt,map}}$	$C_{\text{opt,map}}$	$K_{\text{opt,analytical}}$	$C_{\text{opt,analytical}}$
Reg.1	0.625	0.01	3720	18	3717	9
Reg.2	0.8	0.02	2290	34	2302	20
Reg.3	1	0.0075	1530	30	1534	21

approach to approximate the radiation convolution integral. Combining Eqs. (22) and (26), the system of equations for the fully submerged point absorber heaving in the x-direction reads as

$$(m + A_\infty)\ddot{x}(t) + \boldsymbol{C}_{\text{r}}\boldsymbol{\zeta}_{\text{r}}(t) = f_{\text{w}}(t) + f_{\text{v}}(t) - Kx(t) - C\dot{x}(t), \quad (27)$$

$$\dot{\boldsymbol{\zeta}}_{\text{r}}(t) = \boldsymbol{\mathcal{A}}_{\text{r}}\boldsymbol{\zeta}_{\text{r}}(t) + \boldsymbol{\mathcal{B}}_{\text{r}}\dot{x}(t). \quad (28)$$

The viscous drag force in Eq. (27) is modeled using a Morrison formulation as

$$f_{\text{v}}(t) = -\frac{1}{2}\rho_{\text{w}}C_{\text{d}}S_x|\dot{x}|\dot{x}, \quad (29)$$

in which $\rho_{\text{w}} = 1025$ kg/m^3 is the density of sea water, C_{d} is the drag coefficient, and S_x is the planar cross-sectional area normal to the force.

We use linear potential flow theory to compute the wave excitation force f_{w} on the submerged point absorber. Both regular and irregular sea states are considered in this work. The regular waves are characterized by a single wave frequency ω or time period $\mathcal{T} = 2\pi/\omega$, wave height $\mathcal{H}$ or amplitude $a = \mathcal{H}/2$, and wavelength λ or wavenumber $\kappa = 2\pi/\lambda$. The wave frequency and the wavenumber satisfy the dispersion relation[69]

$$\omega^2 = g\kappa\tanh(\kappa d), \quad (30)$$

in which $g = 9.81$ m/s^2 is the acceleration due to gravity and d is the mean depth of water. In contrast, an irregular sea state consists of a large number of regular wave components, each having its own wave amplitude a_i, angular frequency ω_i [or equivalently, wavenumber κ_i obtained from the dispersion relation given by Eq. (30)], and random phase θ_i that is uniformly distributed in the range $[0, 2\pi]$. The linear superposition of regular wave components implies that the energy carried by an irregular wave is the sum of the energy transported by individual wave components. When the number of wave components tends to infinity, a continuous wave spectral density function $S(\omega)$ is used to describe the energy content of the wave components in an infinitesimal frequency bandwidth dω. In this work, we use a JONSWAP[70] spectrum to generate the irregular sea state. The JONSWAP spectrum is characterized by two statistical parameters: significant wave height $\mathcal{H}_{\text{s}}$ and peak period $\mathcal{T}_{\text{p}}$. The amplitude of each wave component is related to the spectral density function

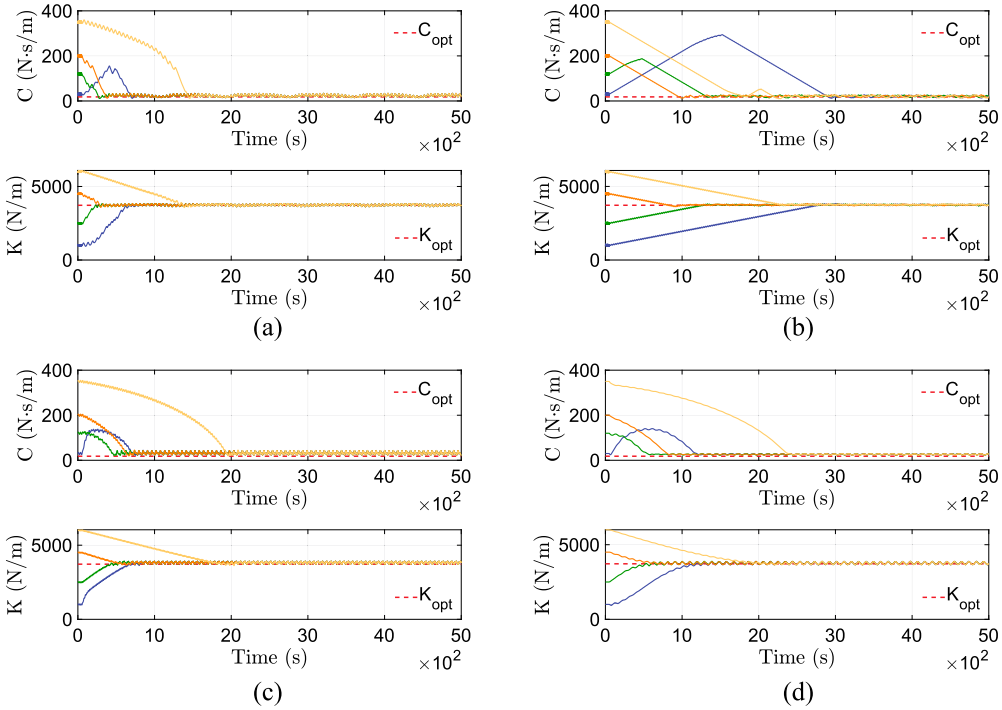

FIG. 15. Optimization of reactive and resistive coefficients, K and C, respectively, for the cylindrical buoy in regular sea state "Reg.1" using (a) sliding mode, (b) relay, (c) LSQ, and (d) perturbation-based ES algorithms. The optimal $K_{\text{opt}} = 3720$ N/m and $C_{\text{opt}} = 18$ N s/m values are indicated by dashed lines in the plots.

by

$$a_i = \sqrt{2 \cdot S(\omega_i) \cdot \Delta\omega}. \tag{31}$$

In a regular sea state, the point absorber system is mathematically equivalent to the mechanical oscillator of Sec. IV A, if one replaces the damping coefficient c with the radiation damping $B(\omega)$, the mass of the oscillator m with the total mass $(m + A(\omega))$, and the spring stiffness k with the hydrostatic stiffness k_{hydro}, which is zero for a fully submerged body. Therefore, using the impedance-matching control theory, the energy-maximizing PTO parameters can be found as

$$K_{\text{opt}} = \omega^2(m + A(\omega)), \tag{32}$$

$$C_{\text{opt}} = B(\omega). \tag{33}$$

We remark that if an additional viscous drag force is included in the equations of motion, as done in this work, then the optimal PTO resistive coefficient C_{opt} would be higher than $B(\omega)$ as shown by Beatty *et al.*.[71] We make use of Eqs. (32) and (33) to verify the results of ES algorithms.

For an irregular sea state, the optimal PTO parameters cannot be found analytically as multiple frequencies are present in the point absorber velocity $\dot{x}$ (and other state variables), which is used to evaluate the $\bar{P}$ expression in Eq. (17). Therefore, to verify the optimal solution obtained from ES algorithms, we create a performance map of the system using a brute-force search of parametric space.

1. Device and wave characteristics

Motivated by our prior work on numerical modeling of a fully submerged axisymmetric point absorber device,[72] we simulate a two-dimensional cylindrical and a three-dimensional spherical buoy to perform extremum-seeking control simulations. Both devices have the same diameter $D = 0.16$ m and a homogeneous mass density of $\rho_s = 922.5$ kg/m^3. Their depth of submergence is taken to be $d_s = 0.25$ m, and the mean depth of water is taken as $d = 0.65$ m. Table I tabulates the regular and irregular sea states simulated in this work. These wave characteristics are chosen based on the scale of the device; see Ref. 72 and Ref. 73 for discussion.

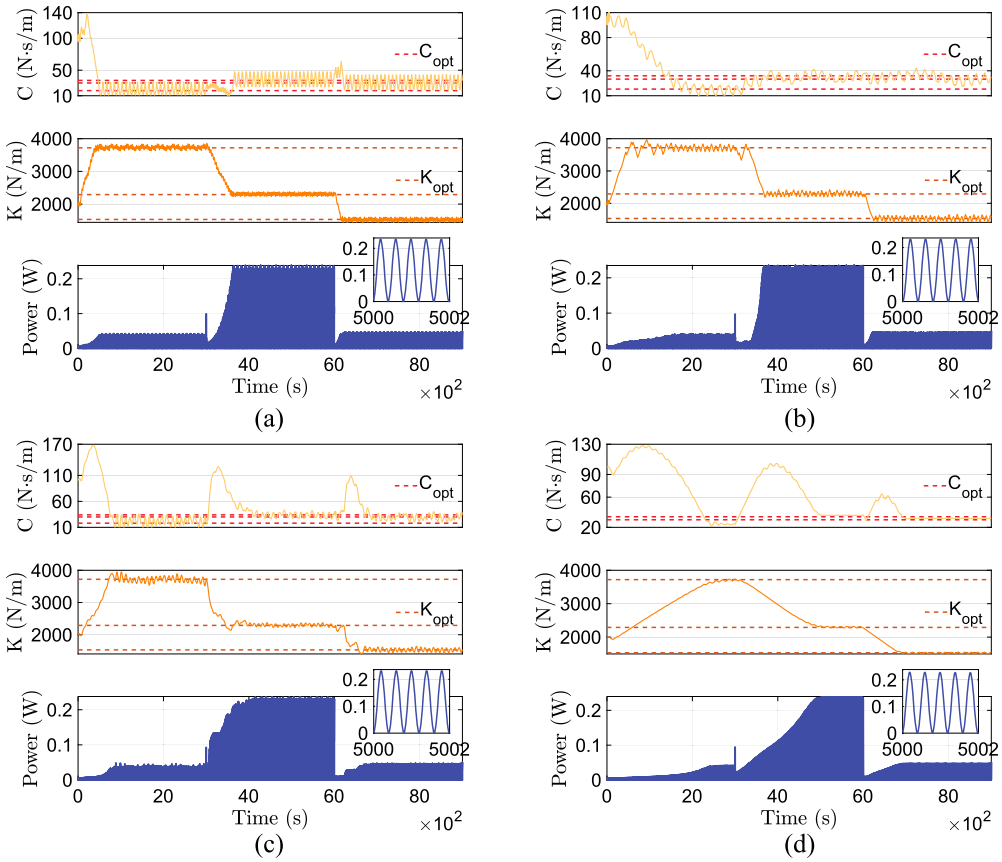

FIG. 16. Optimization of reactive and resistive coefficients, K and C, respectively, for the cylindrical buoy subject to changing sea states using (a) sliding mode, (b) relay, (c) LSQ, and (d) perturbation-based ES algorithms. The optimal K_{opt} and C_{opt} values in three different sea states from Table III are indicated by dashed lines in the plots.

TABLE IV. Optimal PTO coefficients for a two-dimensional cylindrical buoy subject to irregular waves using impedance-matching control theory and through a brute-force search. Units: $\mathcal{T}_p$ is in s, $\mathcal{H}_s$ is in m, K is in N/m, and C is in N s/m.

Sea state ID	$\mathcal{T}_p$	$\mathcal{H}_s$	$K_{opt,map}$	$C_{opt,map}$
Irreg.1	0.625	0.01	3440	32
Irreg.2	0.8	0.02	2170	44
Irreg.3	1	0.0075	1480	40

V. RESULTS

In this section, results are presented for energy-maximizing K and C PTO coefficients using different ES schemes. For each considered system, we present the results for a two-parameter optimization problem, in which both K and C parameters are simultaneously optimized. In some cases, the results for a single-parameter optimization problem, in which either K or C is optimized, are also presented.

A. Mass-spring-damper system

The mass-spring-damper system of Sec. IV A is considered here using the parameters tabulated in Table II. The table also lists the optimal values of K_{opt} and C_{opt} coefficients, obtained analytically. We begin with single-parameter optimization of either reactive coefficient K or resistive coefficient C by keeping the other fixed at its optimal value. The optimization results for K with different initial values are shown in Fig. 10. As can be seen in the figure, all ES algorithms converge to the theory-predicted optimal value. Similar trends are obtained for the optimization results for C, which are shown in Fig. 20 in Appendix B.

Next, we perform simultaneous optimization of both PTO coefficients. The results are shown in Fig. 11 for four ES algorithms; the self-driving ES method did not converge reliably for the two-parameter optimization problem (divergent data not presented). Based on the results obtained in this section, we make some remarks about different algorithms:

- The sliding mode ES proved quite robust and did not require re-tuning of parameters for varying conditions such as the frequency and/or amplitude of the external force. Moreover, the number of parameters to tune is relatively small. A drawback of the scheme is that the steady-state solution oscillates near the optima, as shown in Fig. 10(a). This, however, results in a negligible variation in the PTO power, as shown in Fig. 12, which compares the extracted power as a function of time using perturbation-based and sliding mode ES methods. The former controller produces negligible oscillation in the steady-state solution of the K coefficient.

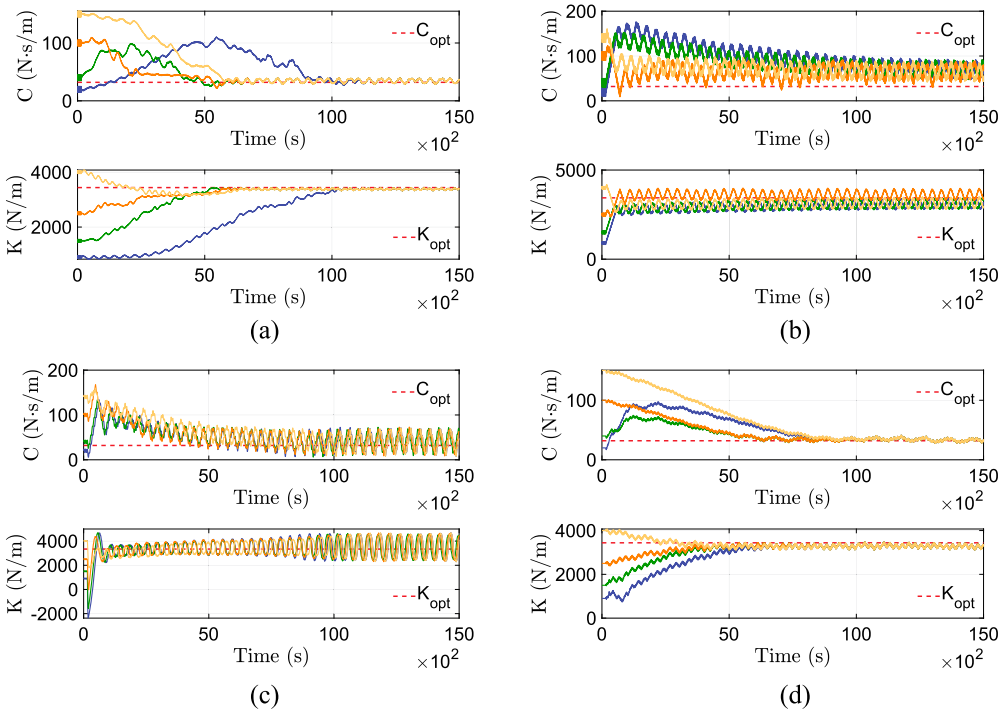

FIG. 17. Optimization of reactive and resistive coefficients, K and C, respectively, for the cylindrical buoy operating in the irregular sea state "Irreg.1" using (a) sliding mode, (b) relay, (c) LSQ, and (d) perturbation-based ES algorithms. The optimal K_{opt} = 3440 N/m and C_{opt} = 32 N s/m values are indicated by dashed lines in the plots.

- The self-driving ES achieves convergence to the optimal value without steady-state oscillations. It is relatively robust, but the main drawback includes tuning of a large number of parameters. In addition, it did not converge reliably for the multi-parameter optimization problem using the algorithm described in Sec. III D.
- The relay ES is also relatively insensitive to the frequency and/or amplitude variation of the external force. It is simple to tune as well. However, it also results in steady-state oscillations in the solution.
- The LSQ-ES proved more robust than the relay ES, having roughly the same number of parameters to tune. It also results in less oscillations in the steady-state solution compared to the relay ES, although they are not completely eliminated.
- Perturbation-based ES is one of the more popular ES schemes used in the literature. The main advantage of this method is its stability, although the choice of cutoff frequencies of the filters largely dictates its performance. The method can achieve a controlled amount of oscillation in the converged solution, as shown in Figs. 10(e), 20(e), and 11(d). The rate of convergence of this method also depends upon the frequency of the external perturbation signal used to estimate the gradient.

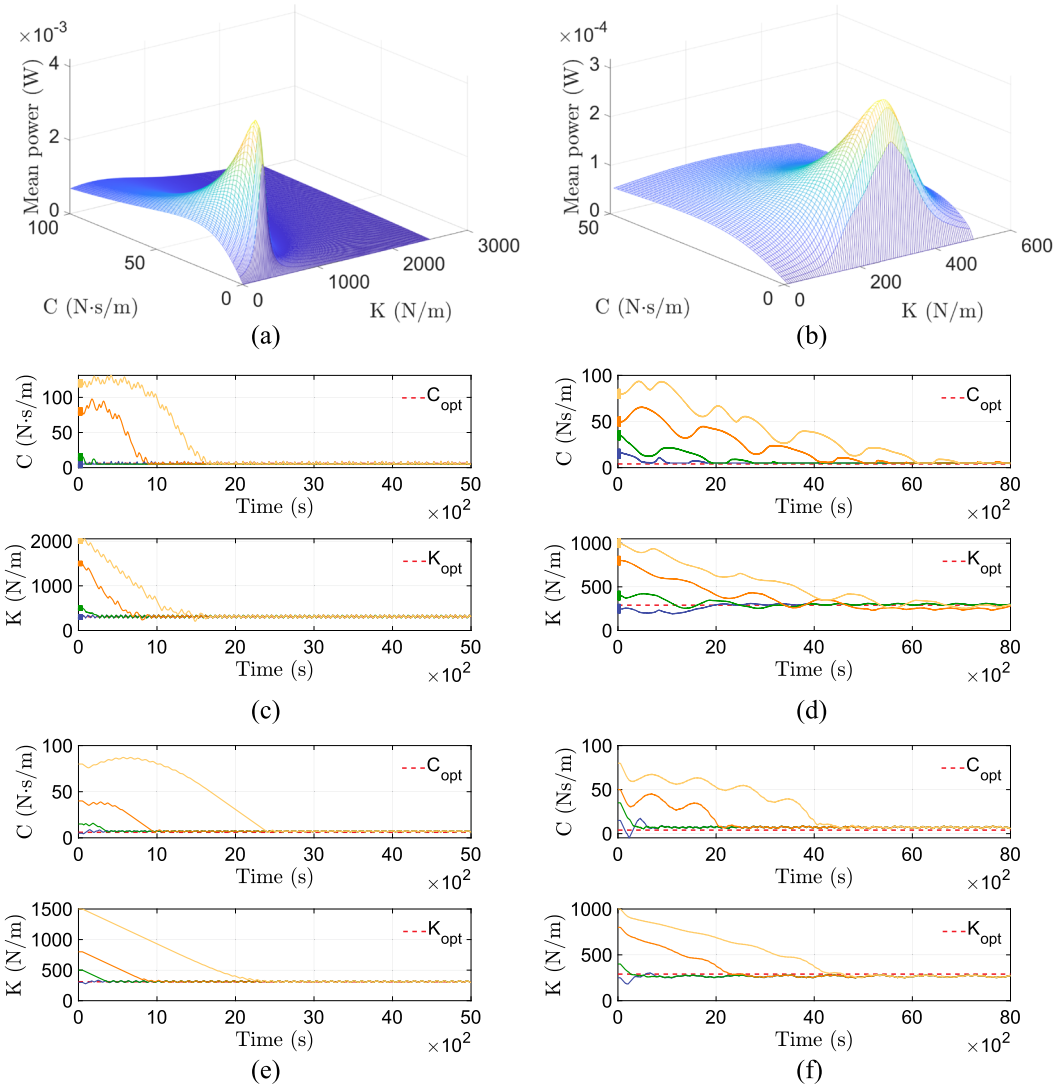

FIG. 18. Optimization of reactive and resistive coefficients, K and C, respectively, for the spherical buoy operating in regular and irregular sea states "Reg.1" and "Irreg.1" using sliding mode [(c) and (d)] and perturbation-based [(e) and (f)] ES algorithms. For sea state "Reg.1," the optimal PTO coefficients are $K_{opt,map}$ = 310 N/m and $C_{opt,map}$ = 6 N s/m; see (a). The optimal PTO coefficients for sea state "Irreg 1" are $K_{opt,map}$ = 290 N/m and $C_{opt,map}$ = 4 N s/m; see (b).

B. Cylindrical point absorber

1. ES performance in a regular sea state

Next, we consider a two-dimensional cylindrical buoy of Sec. IV B 1 subject to regular waves. Three regular waves of different heights and time periods are considered (Table I). Figure 13 plots the frequency-dependent added mass $A(\omega)$ and frequency-dependent radiation damping $B(\omega)$ for the two-dimensional cylinder; the plotted values can be used to estimate the optimal reactive and resistive coefficients of the PTO mechanism, using Eqs. (32) and (33), respectively. Since the theoretical formula ignores the viscous drag force, we perform a brute-force search of the parametric space to find the optimal values of the resistive coefficient. Figure 14 plots the power vs coefficient reference-to-output map, and Table III lists their optimal values for three different sea states. The tabulated values confirm that the theoretical estimates of the optimal reactive coefficients are quite accurate, whereas the optimal resistive coefficients are under-predicted.

Figure 15 shows the convergence history of K and C coefficients using four ES algorithms for the regular sea state "Reg.1." As can be seen in the figure, all four algorithms converge to the optimum values of the PTO coefficients. Moreover, their convergence behavior is similar to the mechanical oscillator problem of Sec. IV A. Similar to the mass-spring-damper case, the self-driving ES method did not converge for the two-parameter optimization problem. However, oscillation-free steady-state solutions are obtained, when self-driving ES is used to optimize either K or C. The single-parameter optimization results obtained using the self-driving ES method are shown in Fig. 21 in Appendix C.

Next, we test the adaptive capability of ES algorithms. Starting with sea state "Reg.1," the wave conditions for the cylindrical buoy are changed to "Reg.2" and then subsequently to "Reg.3." Figure 16 shows that all four ES algorithms can reliably adapt to the changing wave conditions and adjust the PTO coefficients automatically to achieve optimal performance in each sea state. The results also confirm that extremum-seeking control algorithms do not require any wave forecasting/prediction information to attain the optimum. Indeed, the performance function used in the extremum-seeking algorithm requires only on-board instrumentation to estimate the absorbed PTO power. Thus, ES can be used as a *causal* controller for WECs.

2. ES performance in an irregular sea state

A WEC device subject to irregular waves has multiple frequencies in its dynamics. Consequently, a closed-form solution for energy-maximizing PTO coefficients is difficult to obtain analytically. To verify the controller results, we perform a brute-force search of the parametric space to find the optimal values of the PTO coefficients for three irregular sea states. Figure 22 in Appendix D plots the power vs PTO coefficient reference-to-output map, and Table IV lists their optimal values.

Figure 17 shows the convergence history of K and C coefficients using four ES algorithms for the sea state "Irreg.1." From the figure, it can be seen that the sliding mode and perturbation-based ES methods outperform the relay and LSQ-ES algorithms. The latter two methods display large oscillations in the steady-state solution. Between the relay and LSQ methods, the former has a better convergence rate. This can be attributed to the fact that the relay ES algorithm does not use the magnitude of the performance gradient, which is noisier compared to its regular sea state counterpart when computed through data buffers. However, for regular waves, LSQ-ES convergence is better compared to the relay ES scheme because a more accurate gradient is available in this case; see Fig. 15. Similar results are obtained for sea states "Irreg.2" and "Irreg.3" and are shown in Figs. 23 and 24, respectively, in Appendix D.

C. Spherical point absorber

Intuitively speaking, as we employ model-free ES schemes to optimize mechanical oscillators in this work, a particular device geometry should not matter for the algorithmic success. However, to verify that the model-free ES algorithms also converge for a different device geometry (and consequently, for a different hydrodynamical system), we perform ES optimization of a spherical buoy described in Sec. IV B 1. Sea states "Reg.1" and "Irreg.1" are considered for the sliding mode and perturbation-based ES algorithms.

Figure 18 shows the convergence history of PTO coefficients K and C using sliding mode ES (middle row) and perturbation-based ES (bottom row) algorithms. As can be seen in the figure, steady-state convergence toward the performance-optimal solution is achieved with both algorithms (convergence data not shown for relay and LSQ schemes for brevity). The optimal values obtained from the ES optimization can be confirmed from power vs PTO coefficient reference-to-output maps (top row).

VI. CONCLUSIONS

In this study, we systematically investigated the feasibility of ES control optimization for wave energy converters to improve their conversion efficiency. Five different ES schemes were tested for heaving WECs: (i) sliding mode ES, (ii) relay ES, (iii) least-squares gradient ES, (iv) self-driving ES, and (v) perturbation-based ES. The optimization problem of wave energy absorption in WECs was formulated in terms of finding the optimal PTO coefficients. Alternatively, the ES optimization problem can also be formulated in terms of finding the optimal PTO force directly, as typically done in model predictive control (MPC) of WECs.[31] Direct optimization of PTO force using ES control is deferred to future endeavors.

The performance function for the ES control was defined as the energy absorbed by the PTO system over a given period of time, which could be measured through on-board instrumentation, and does not require any wave measurements. This implies that the model-free ES can be used as a *causal* controller for WECs. The optimization results were verified against analytical solutions and the extremum of reference-to-output maps. The numerical results demonstrate that except for the self-driving ES algorithm, the other four ES schemes reliably converge for the two-parameter optimization problem. The self-driving ES is more suitable for optimizing a single parameter of the problem or when the objective is to find the optimal control force directly, rather than to optimize the gains of the control law. An advantage of the self-driving ES scheme is that it leads to an oscillation-free steady-state solution. The results also show that for an irregular sea state, the sliding mode and

perturbation-based ES schemes have better convergence to the optimum in comparison to the other ES schemes. The least-squares ES scheme performs better than the relay ES scheme, whenever the gradient estimation through data acquisition is smooth and accurate. This can be concluded by comparing the convergence history of LSQ-ES and relay ES for regular and irregular sea states; LSQ performed better than relay in the case of regular waves, and the converse is true for irregular waves. For all ES schemes, the convergence of PTO coefficients toward the performance-optimal values is tested for widely different initial values, in order to avoid bias toward the extremum. We also demonstrated the adaptive capability of ES control by considering a case in which the ES controller adapts to the new extremum automatically amid changes in the simulated wave conditions.

All extremum-seeking schemes achieve optimum within a single simulation. This allows for a possibility of using model-free ES algorithms within a nonlinear computational fluid dynamics (CFD) framework to simulate wave–structure interaction of WECs. In the CFD literature, evolution-based optimization strategies (e.g., genetic algorithm) are predominantly used for solving optimization problems. However, such evolutionary strategies typically require a large number of function evaluations, which can be prohibitively expensive for fully resolved wave–structure interaction problems.[73,74] We shall consider such an approach in the future.

ACKNOWLEDGMENTS

A.P.S.B. and P.N. acknowledge helpful discussions with Miroslav Krstić over the course of this work. A.P.S.B. acknowledges Nishant Nangia for carefully reading the manuscript and providing helpful comments.

APPENDIX A: POWER COMPONENTS IN PERFORMANCE FUNCTION

Here, we numerically verify that including the reactive component of power in the performance function does not affect the

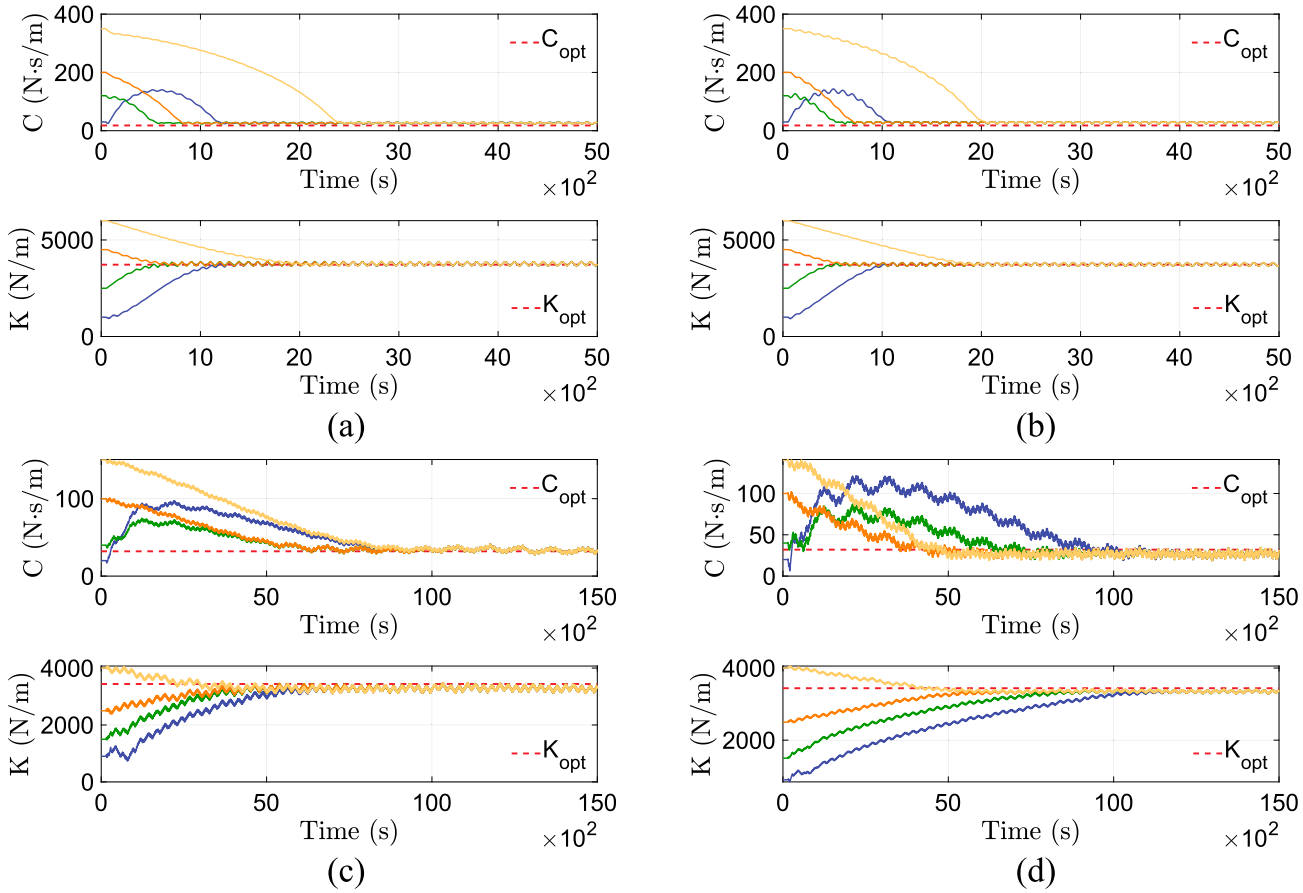

FIG. 19. Optimization of reactive and resistive coefficients, K and C, respectively, for the cylindrical buoy in regular "Reg.1" [top row (a) and (b)] and irregular "Irreg.1" [bottom row (c) and (d)] waves using different power components in the performance function. The optimal K_{opt} = 3720 N/m and C_{opt} = 18 N s/m values for regular waves and K_{opt} = 3440 N/m and C_{opt} = 32 N s/m values for irregular waves are indicated by dashed lines in the plots.

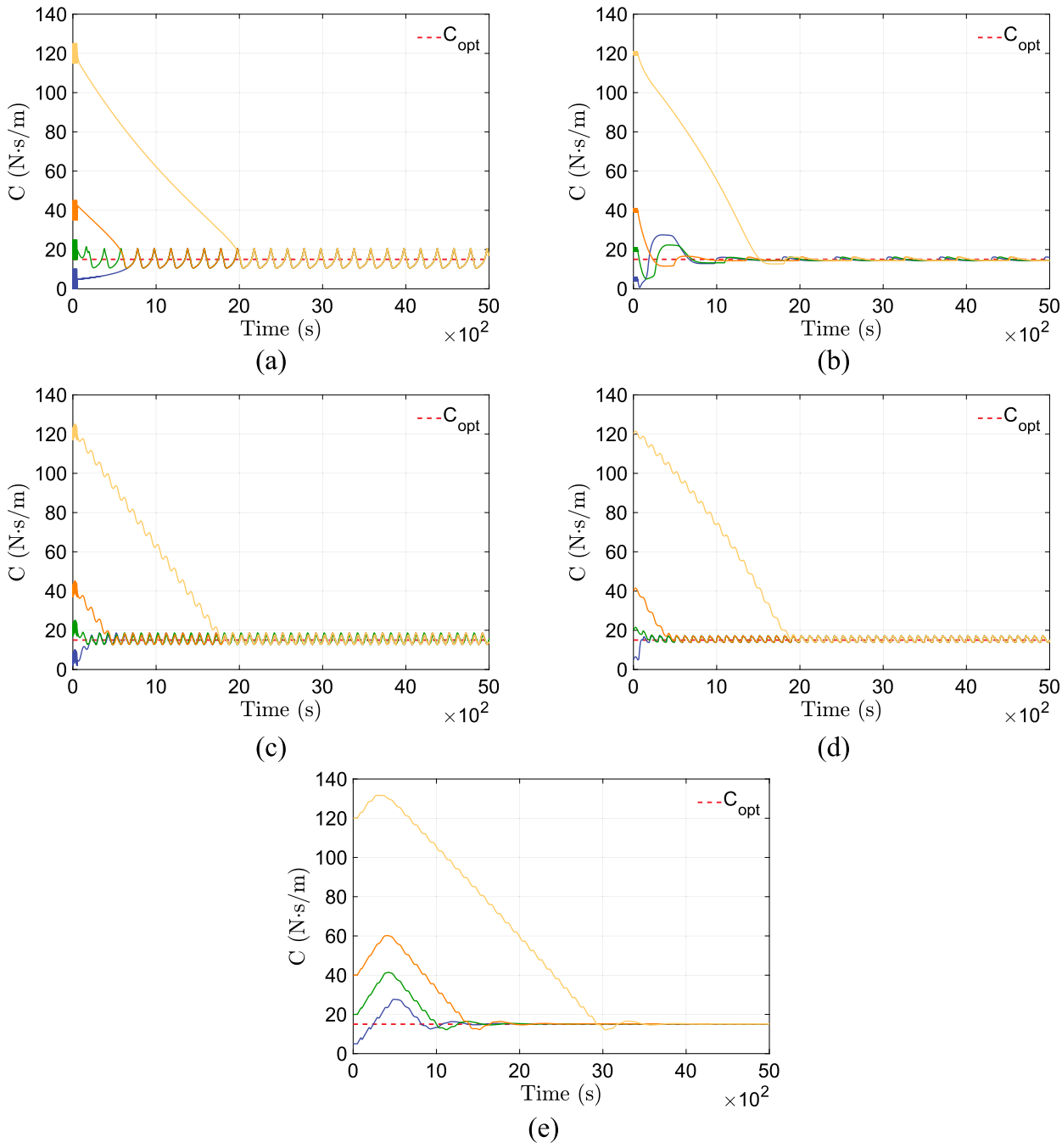

FIG. 20. Optimization of the resistive coefficient C at a fixed value of reactive coefficient $K = K_{opt}$ for the mass-spring-damper system using (a) sliding mode, (b) self-driving, (c) relay, (d) LSQ, and (e) perturbation-based ES algorithms. The optimal C_{opt} = 15 N s/m value is indicated by the dashed line in the plots.

optimal values of the PTO coefficients obtained using an ES control scheme. We demonstrate this by comparing results in Fig. 19 for the cylindrical buoy subject to regular and irregular waves of the type "Reg.1" and "Irreg.1," respectively. The perturbation-based ES method is used here. As can be seen in the figure, the inclusion of the reactive power term in the performance function does not affect the final outcome of the optimization. This was also demonstrated theoretically in Eq. (21).

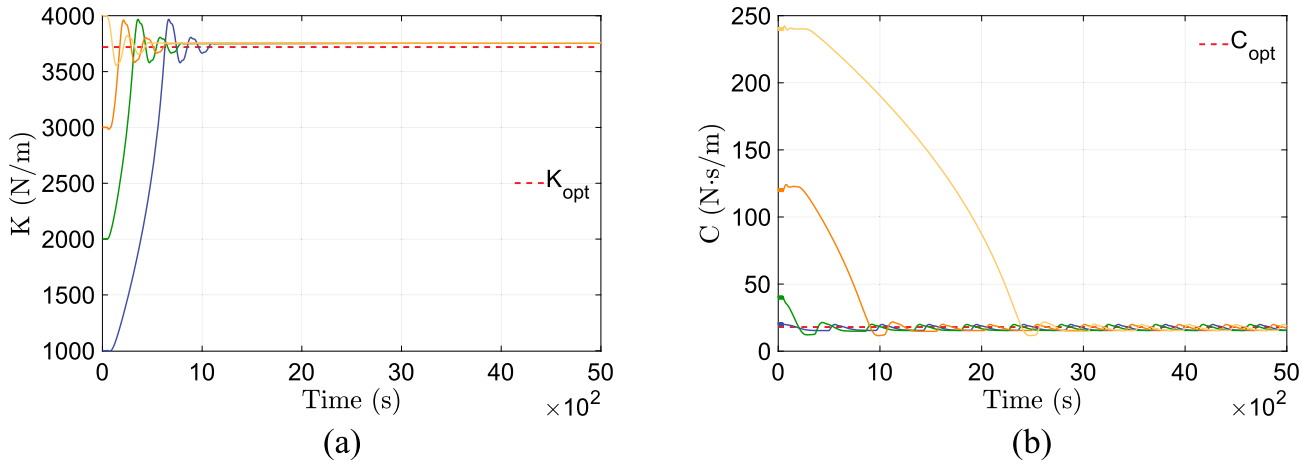

FIG. 21. Optimization of the (a) reactive PTO coefficient K and (b) resistive PTO coefficient C using the self-driving ES algorithm for a cylindrical buoy in the regular sea state "Reg.1." The optimal K_{opt} = 3720 N/m and C_{opt} = 18 N s/m values are indicated by dashed lines in the plots.

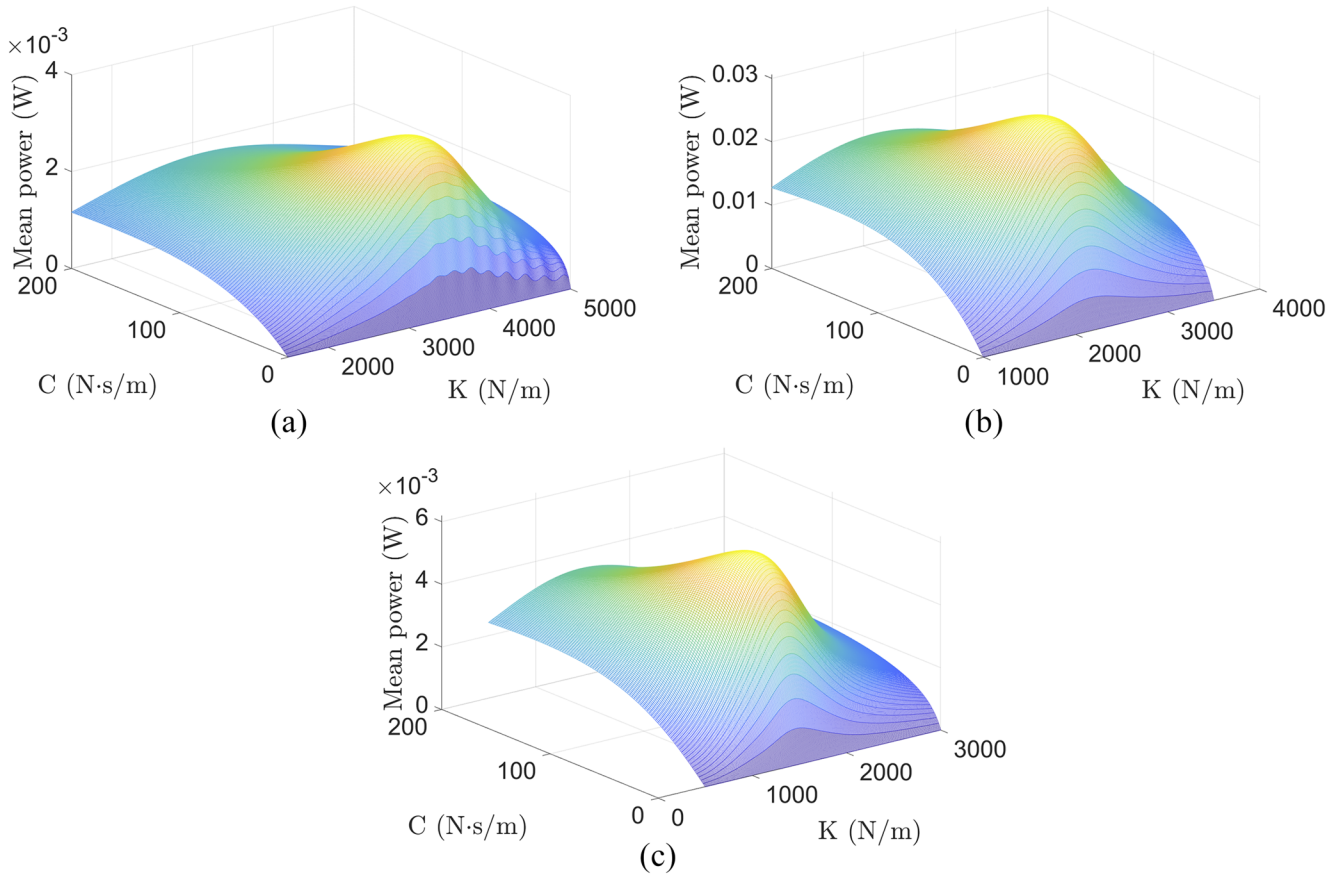

FIG. 22. Power vs PTO coefficient reference-to-output map for a two-dimensional cylinder operating in an irregular sea state. The optimal PTO coefficients are (a) K_{opt} = 3440 N/m and C_{opt} = 32 N s/m; (b) K_{opt} = 2170 N/m and C_{opt} = 44 N s/m; and (c) K_{opt} = 1480 N/m and C_{opt} = 40 N s/m.

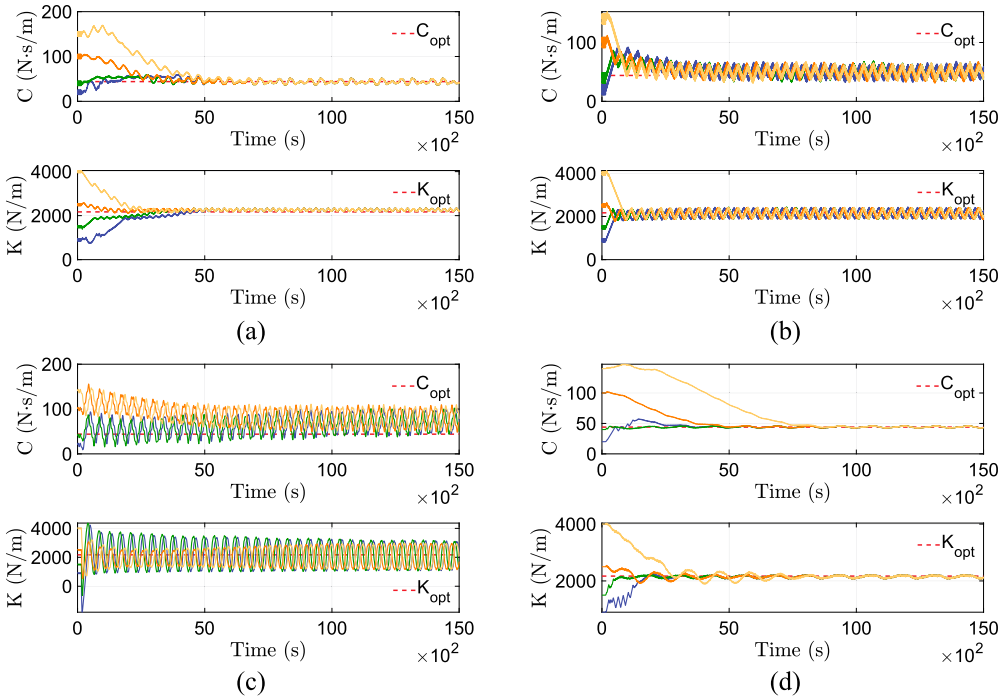

FIG. 23. Optimization of reactive and resistive coefficients, K and C, respectively, for the cylindrical buoy operating in the irregular sea state "Irreg.2" using (a) sliding mode, (b) relay, (c) LSQ, and (d) perturbation-based ES algorithms. The optimal K_{opt} = 2170 N/m and C_{opt} = 44 N s/m values are indicated by dashed lines in the plots.

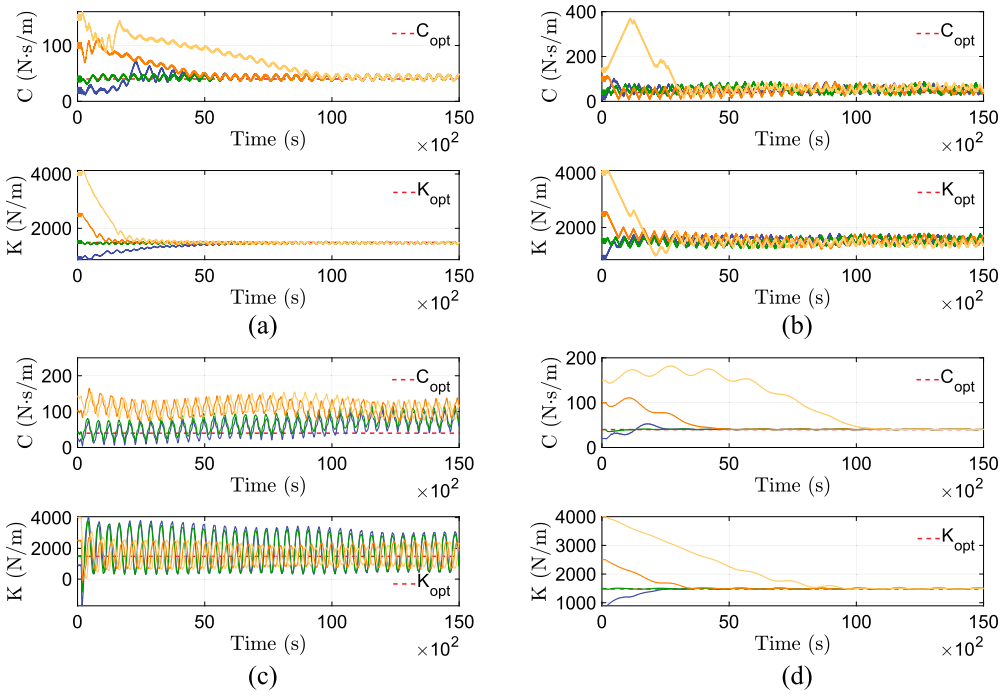

FIG. 24. Optimization of reactive and resistive coefficients, K and C, respectively, for the cylindrical buoy operating in the irregular sea state "Irreg.3" using (a) sliding mode, (b) relay, (c) LSQ, and (d) perturbation-based ES algorithms. The optimal K_{opt} = 1480 N/m and C_{opt} = 40 N s/m values are indicated by dashed lines in the plots.

APPENDIX B: OPTIMIZATION OF DAMPING COEFFICIENT C FOR MASS-SPRING-DAMPER SYSTEM

Here, we present the optimization results for C at a fixed value of reactive coefficient $K = K_{opt}$ for the mass-spring-damper system using different ES algorithms, as considered in Sec. V A.

APPENDIX C: SELF-DRIVING ES OPTIMIZATION FOR A CYLINDRICAL POINT ABSORBER IN REGULAR SEA STATE "REG.1"

Here, the single parameter optimization results obtained using self-driving ES for a two-dimensional cylindrical buoy operating in regular sea state "Reg.1" (as considered in Sec. V B 1) are presented.

APPENDIX D: IRREGULAR SEA STATES "IRREG.2" AND "IRREG.3" FOR CYLINDRICAL POINT ABSORBER

Here, the power vs PTO coefficient reference-to-output map and optimization results for a two-dimensional cylindrical buoy operating in an irregular sea state (as considered in Sec. V B 2) are presented.

DATA AVAILABILITY

The data that support the findings of this study are openly available in the GitHub repository at https://github.com/amneetb/extremum-seeking-wecs.

REFERENCES

[1] D. Evans, D. Jeffrey, S. Salter, and J. Taylor, "Submerged cylinder wave energy device: Theory and experiment," Appl. Ocean Res. **1**(1), 3–12 (1979).
[2] U.S. Department of Energy, Revolution Now, https://www.energy.gov/revolution-now, 2013.
[3] K. Gunn and C. Stock-Williams, "Quantifying the global wave power resource," Renewable Energy **44**, 296–304 (2012).
[4] B. Czech and P. Bauer, "Wave energy converter concepts: Design challenges and classification," IEEE Ind. Electron. Mag. **6**(2), 4–16 (2012).
[5] A. Babarit, *Ocean Wave Energy Conversion: Resource, Technologies and Performance* (Elsevier, 2017).
[6] J. V. Ringwood, G. Bacelli, and F. Fusco, "Energy-maximizing control of wave-energy converters: The development of control system technology to optimize their operation," IEEE Control Syst. Mag. **34**(5), 30–55 (2014).
[7] J. V. Ringwood, G. Bacelli, and F. Fusco, "Control, forecasting and optimisation for wave energy conversion," IFAC Proc. Vol. **47**(3), 7678–7689 (2014).
[8] A. Maria-Arenas, A. J. Garrido, E. Rusu, and I. Garrido, "Control strategies applied to wave energy converters: State of the art," Energies **12**(16), 3115 (2019).
[9] M. Krstić and H.-H. Wang, "Stability of extremum seeking feedback for general nonlinear dynamic systems," Automatica **36**(4), 595–601 (2000).
[10] A. Banaszuk, Y. Zhang, and C. A. Jacobson, "Adaptive control of combustion instability using extremum-seeking," in *Proceedings of the 2000 American Control Conference (ACC) (IEEE Cat. No. 00CH36334)* (IEEE, 2000), Vol. 1, pp. 416–422.
[11] P. Binetti, K. B. Ariyur, M. Krstic, and F. Bernelli, "Formation flight optimization using extremum seeking feedback," J. Guid., Control, Dyn. **26**(1), 132–142 (2003).
[12] Y. Li, M. A. Rotea, G.-C. Chiu, L. G. Mongeau, and I.-S. Paek, "Extremum seeking control of a tunable thermoacoustic cooler," IEEE Trans. Control Syst. Technol. **13**(4), 527–536 (2005).
[13] C. Zhang, A. Siranosian, and M. Krstić, "Extremum seeking for moderately unstable systems and for autonomous vehicle target tracking without position measurements," Automatica **43**(10), 1832–1839 (2007).
[14] M. Bagheri, M. Krstić, and P. Naseradinmousavi, "Multivariable extremum seeking for joint-space trajectory optimization of a high-degrees-of-freedom robot," J. Dyn. Syst., Meas., Control **140**(11), 111017 (2018).
[15] L. Luo and E. Schuster, "Mixing enhancement in 2D magnetohydrodynamic channel flow by extremum seeking boundary control," in *2009 American Control Conference* (IEEE, 2009), pp. 1530–1535.
[16] I. Munteanu, A. I. Bratcu, and E. Ceangă, "Wind turbulence used as searching signal for MPPT in variable-speed wind energy conversion systems," Renewable Energy **34**(1), 322–327 (2009).
[17] D. Shen, P. Khayyer, and A. Izadian, "Sliding mode extremum seeking control for maximum power point tracking in wind system," in *2016 IEEE Power and Energy Conference at Illinois (PECI)* (IEEE, 2016), pp. 1–6.
[18] L. Hu, F. Xue, Z. Qin, J. Shi, W. Qiao, W. Yang, and T. Yang, "Sliding mode extremum seeking control based on improved invasive weed optimization for MPPT in wind energy conversion system," Appl. Energy **248**, 567–575 (2019).
[19] S. L. Brunton, C. W. Rowley, S. R. Kulkarni, and C. Clarkson, "Maximum power point tracking for photovoltaic optimization using extremum seeking," in *2009 34th IEEE Photovoltaic Specialists Conference (PVSC)* (IEEE, 2009), pp. 000013–000016.
[20] H. Zazo, E. Del Castillo, J. F. Reynaud, and R. Leyva, "MPPT for photovoltaic modules via Newton-like extremum seeking control," Energies **5**(8), 2652–2666 (2012).
[21] A. Kebir, L. Woodward, and O. Akhrif, "Extremum-seeking control with adaptive excitation: Application to a photovoltaic system," IEEE Trans. Ind. Electron. **65**(3), 2507–2517 (2017).
[22] P. B. Garcia-Rosa, F. Lizarralde, and S. F. Estefen, "Optimization of the wave energy absorption in oscillating-body systems using extremum seeking approach," in *2012 American Control Conference (ACC)* (IEEE, 2012), pp. 1011–1016.
[23] J. Hals, J. Falnes, and T. Moan, "A comparison of selected strategies for adaptive control of wave energy converters," J. Offshore Mech. Arct. Eng. **133**(3), 031101 (2011).
[24] M. Leblanc, "Sur l'electrification des chemins de fer au moyen de courants alternatifs de frequence elevee," Rev. Gen. Electr. **12**(8), 275–277 (1922).
[25] V. Kazakevich, *On Extremum Seeking* (Moscow High Technical University, 1944).
[26] Y. Pan, Ü. Özgüner, and T. Acarman, "Stability and performance improvement of extremum seeking control with sliding mode," Int. J. Control **76**(9-10), 968–985 (2003).
[27] C. Olalla, M. I. Arteaga, R. Leyva, and A. El Aroudi, "Analysis and comparison of extremum seeking control techniques," in *2007 IEEE International Symposium on Industrial Electronics* (IEEE, 2007), pp. 72–76.
[28] B. Hunnekens, M. Haring, N. van de Wouw, and H. Nijmeijer, "A dither-free extremum-seeking control approach using 1st-order least-squares fits for gradient estimation," in *53rd IEEE Conference on Decision and Control* (IEEE, 2014), pp. 2679–2684.
[29] M. A. Haring, "Extremum-seeking control: Convergence improvements and asymptotic stability," Ph.D. thesis (Institutt for Teknisk Kybernetikk, 2016); available at https://ntnuopen.ntnu.no/ntnu-xmlui/handle/11250/2394949.
[30] G. Vissio, D. Valério, G. Bracco, P. Beirão, N. Pozzi, and G. Mattiazzo, "ISWEC linear quadratic regulator oscillating control," Renewable Energy **103**, 372–382 (2017).
[31] N. Faedo, S. Olaya, and J. V. Ringwood, "Optimal control, MPC and MPC-like algorithms for wave energy systems: An overview," IFAC J. Syst. Control **1**, 37–56 (2017).
[32] J. Rabault, M. Kuchta, A. Jensen, U. Réglade, and N. Cerardi, "Artificial neural networks trained through deep reinforcement learning discover control strategies for active flow control," J. Fluid Mech. **865**, 281–302 (2019).
[33] J. Rabault and A. Kuhnle, "Accelerating deep reinforcement learning strategies of flow control through a multi-environment approach," Phys. Fluids **31**, 094105 (2019).
[34] H. Tang, J. Rabault, A. Kuhnle, Y. Wang, and T. Wang, "Robust active flow control over a range of Reynolds numbers using an artificial neural network trained through deep reinforcement learning," Phys. Fluids **32**, 053605 (2020).
[35] T. Duriez, S. Brunton, and B. Noack, *Machine Learning Control: Taming Nonlinear Dynamics and Turbulence* (Springer, 2016), Vol. 116.

[36]S. Brunton and B. Noack, "Closed-loop turbulence control: Progress and challenges," Appl. Mech. Rev. **67**, 050801 (2015).
[37]C. Raibaudo, P. Zhong, B. Noack, and R. Martinuzzi, "Machine learning strategies applied to the control of a fluidic pinball," Phys. Fluids **32**, 015108 (2020).
[38]S. Verma, G. Novati, and P. Koumoutsakos, "Efficient collective swimming by harnessing vortices through deep reinforcement learning," Proc. Natl. Acad. Sci. U. S. A. **115**, 5849–5854 (2018).
[39]E. Anderlini, D. Forehand, E. Bannon, Q. Xiao, and M. Abusara, "Reactive control of a two-body point absorber using reinforcement learning," Ocean Eng. **148**, 650–658 (2017).
[40]E. Anderlini, D. Forehand, P. Stansell, Q. Xiao, and M. Abusara, "Control of a point absorber using reinforcement learning," IEEE Trans. Sustainable Energy **7**, 1681–1690 (2016).
[41]E. Anderlini, D. Forehand, E. Bannon, and M. Abusara, "Control of a realistic wave energy converter model using least-squares policy iteration," IEEE Trans. Sustainable Energy **8**, 1618–1628 (2017).
[42]E. Anderlini, D. Forehand, E. Bannon, and M. Abusara, "Reactive control of a wave energy converter using artificial neural networks," Int. J. Mar. Energy **19**, 207–220 (2017).
[43]S. Thomas, M. Giassi, M. Eriksson, M. Göteman, J. Isberg, E. Ransley, M. Hann, and J. Engström, "A model free control based on machine learning for energy converters in an array," Big Data Cognit. Comput. **2**, 36 (2018).
[44]S. Brunton, B. Noack, and P. Koumoutsakos, "Machine learning for fluid mechanics," Annu. Rev. Fluid Mech. **52**, 477–508 (2020).
[45]K. B. Ariyur and M. Krstic, *Real-Time Optimization by Extremum-Seeking Control* (John Wiley & Sons, 2003).
[46]C. Zhang and R. Ordóñez, *Extremum-Seeking Control and Applications: A Numerical Optimization-Based Approach* (Springer Science & Business Media, 2011).
[47]N. van de Wouw, M. Haring, and D. Nešić, "Extremum-seeking control for periodic steady-state response optimization," in *2012 IEEE 51st IEEE Conference on Decision and Control (CDC)* (IEEE, 2012), pp. 1603–1608.
[48]M. Haring, N. Van De Wouw, and D. Nešić, "Extremum-seeking control for nonlinear systems with periodic steady-state outputs," Automatica **49**(6), 1883–1891 (2013).
[49]M. A. Rotea, "Analysis of multivariable extremum seeking algorithms," in *Proceedings of the 2000 American Control Conference (ACC) (IEEE Cat. No. 00CH36334)* (IEEE, 2000), Vol. 1, pp. 433–437.
[50]G. C. Walsh, "On the application of multi-parameter extremum seeking control," in *Proceedings of the 2000 American Control Conference (ACC) (IEEE Cat. No. 00CH36334)* (IEEE, 2000), Vol. 1, pp. 411–415.
[51]A. R. Teel and D. Popovic, "Solving smooth and nonsmooth multivariable extremum seeking problems by the methods of nonlinear programming," in *Proceedings of the 2001 American Control Conference (Cat. No. 01CH37148)* (IEEE, 2001), Vol. 3, pp. 2394–2399.
[52]K. B. Ariyur and M. Krstic, "Multivariable extremum seeking feedback: Analysis and design," in Procedings of the Mathematical Theory of Networks and Systems, 2002.
[53]F. E. Azar, M. Perrier, and B. Srinivasan, "Real-time global optimization using multiple units," IFAC Proc. Vol. **42**(19), 49–54 (2009).
[54]D. DeHaan and M. Guay, "Extremum-seeking control of state-constrained nonlinear systems," Automatica **41**(9), 1567–1574 (2005).
[55]M. Guay, E. Moshksar, and D. Dochain, "A constrained extremum-seeking control approach," Int. J. Robust Nonlinear Control **25**(16), 3132–3153 (2015).
[56]U. Ciri, S. Leonardi, and M. A. Rotea, "Evaluation of log-of-power extremum seeking control for wind turbines using large eddy simulations," Wind Energy **22**(7), 992–1002 (2019).
[57]S. Chen, L. Wang, K. Ma, and H. Zhao, "A switching-based extremum seeking control scheme," Int. J. Control **90**(8), 1688–1702 (2017).
[58]R. Leyva, C. Alonso, I. Queinnec, A. Cid-Pastor, D. Lagrange, and L. Martinez-Salamero, "MPPT of photovoltaic systems using extremum—Seeking control," IEEE Trans. Aerosp. Electron. Syst. **42**(1), 249–258 (2006).
[59]J. Sternby, "Extremum control system: An area for adaptive control?," in Preprints of Joint American Control Conference, San Francisco, CA, 1980.
[60]B. T. Powell, "Investigation of extremum seeking control for adaptive exercise machines," Ph.D. thesis, Cleveland State University, 2017.
[61]A. Price, C. Dent, and A. Wallace, "Frequency domain techniques for numerical and experimental modelling of wave energy converters," in Proceedings of the 8th European Wave and Tidal Energy Conference (EWTEC), 2009.
[62]K. Bubbar and B. Buckham, "On establishing an analytical power capture limit for self-reacting point absorber wave energy converters based on dynamic response," Appl. Energy **228**, 324–338 (2018).
[63]U. A. Korde and J. Ringwood, *Hydrodynamic Control of Wave Energy Devices* (Cambridge University Press, 2016).
[64]W. Cummins, "The impulse response function and ship motions," Technical report 1661, David Taylor Model Basin, Washington, DC, 1962.
[65]C.-H. Lee, WAMIT Theory Manual, Department of Ocean Engineering, Massachusetts Institute of Technology, 1995.
[66]ANSYS AQWA Theory Manual, 2014.
[67]T. Perez and T. I. Fossen, "Joint identification of infinite-frequency added mass and fluid-memory models of marine structures," Model., Identif. Control **29**(3), 93–102 (2008).
[68]T. Perez and T. I. Fossen, "Time- vs. frequency-domain identification of parametric radiation force models for marine structures at zero speed," Model., Identif. Control **29**(1), 1–19 (2008).
[69]L. H. Holthuijsen, *Waves in Oceanic and Coastal Waters* (Cambridge University Press, 2007).
[70]J. M. J. Journée and W. W. Massie, *Offshore Hydromechanics* (Delft University of Technology, 2001).
[71]S. J. Beatty, M. Hall, B. J. Buckham, P. Wild, and B. Bocking, "Experimental and numerical comparisons of self-reacting point absorber wave energy converters in regular waves," Ocean Eng. **104**, 370–386 (2015).
[72]P. Dafnakis, A. P. S. Bhalla, S. A. Sirigu, M. Bonfanti, G. Bracco, and G. Mattiazzo, "Comparison of wave-structure interaction dynamics of a submerged cylindrical point absorber with three degrees of freedom using potential flow and computational fluid dynamics models," Phys. Fluids **32**, 093307 (2020).
[73]K. Khedkar, N. Nangia, R. Thirumalaisamy, and A. P. S. Bhalla, "The inertial sea wave energy converter (ISWEC) technology: Device-physics, multiphase modeling and simulations," arXiv:2005.06108 (2020).
[74]N. Nangia, N. A. Patankar, and A. P. S. Bhalla, "A DLM immersed boundary method based wave-structure interaction solver for high density ratio multiphase flows," J. Comput. Phys. **398**, 108804 (2019).